DIPLOMA THESIS

Compact Spherical Loudspeaker Array for Variable Sound-Radiation

Michael Kerscher

March 9, 2010

Assessor: Prof. Robert Höldrich

Supervisor: Dr. Franz Zotter

Institute of Electronic Music and Acoustics

University of Music and Performing Arts, Graz

Graz University of Technology

Abstract

In this work a new spherical loudspeaker array is developed that allows variable sound-radiation in all directions, so called spherical beamforming. In addition to the realization of musical and artistic performances, it can be used for room-acoustical measurements. From a mathematical point of view, radiating sound fields can be decomposed into spherical harmonics, which can be played back by the loudspeaker array and hereby reproduce the desired sound field. The few existing spherical loudspeaker arrays in this field of application use a regular design with Platonic solids, which on the one hand show convenient behavior due to their mathematical decomposition, but on the other hand use an inefficiently large number of loudspeakers. In contrast to Platonic solids, this work uses a spherical geometry, which allows irregular arrangements in favor of an optimal arrangement of the loudspeakers. The spherical cabinet developed in this work mounts 16 loudspeakers, which are uniformly distributed over the surface. This arrangement provides controlled playback of the spherical harmonics up to the third order. As the array is designed for mid-frequency range, small dimensions of the sphere and loudspeakers are desirable. Therefore a compromise between compact dimensions and upper and lower cut-off frequencies must be achieved. In parti- cular spatial aliasing should be avoided and a feasible dynamic range shall be enforced by appropiate filtering.

The work starts with the design and construction of the spherical loudspeaker array including amplification, wiring and mounting. Simulations using the so called sphere cap model, which models the distribution of the loudspeakers on the sphere analytically, enable a pre-estimation of the radiation properties. Finally, acoustical measurements with the complete prototype of the array are made to determine the transfer properties of the loudspeakers and their mutual interaction in the all-over system. For system control, an appropriate algorithm using this data is implemented. This control system contains angular and radial filters. As the latter can use unfeasibly high bass-boosts, an appropriate filterbank for limitation is developed.

Zusammenfassung

In dieser Arbeit wird eine neue kugelförmige Lautsprecheranordnung entwickelt, mit der eine variable Schallabstrahlung in alle Raumrichtungen, sog. sphärisches Beamforming, ermöglicht werden soll. Neben der Realisierung von musikalisch-künstlerischen Darbietungen kann ein solches System z.B. für raumakustische Messungen verwendet werden. Mathematisch gesehen bedient man sich der Zerlegung des Schallfeldes in eine Reihe von Kugelharmonischen, welche über die Lautsprecheranordnung wiedergegeben werden und so das gewünschte Schallfeld reproduzieren. Die wenigen existierenden kugelförmigen Lautsprecheranordnungen in diesem Einsatzbereich verwenden als Bauform regelmäßige Platonische Körper, die zwar günstige Eigenschaften bezüglich der mathematischen Zerlegung besitzen, aber zumeist ineffizient viele Lautsprecher benutzen. Im Gegensatz dazu verwendet diese Arbeit eine kugelrunde Bauform, welche auch unregelmäßige Anordnungen zugunsten einer optimalen Anordnung von Lautsprechern zulässt. Ins letztendlich entworfene kugelförmige Gehäuse sind 16 Lautsprecher eingebaut, die gleichmäßig auf der Kugeloberfläche angeordnet sind. Damit lässt sich ein System zur Wiedergabe von Kugelharmonischen bis dritter Ordnung realisieren. Da die Anordnung als Mitteltöner konzipiert wird, sind möglichst kleine Abmessungen der Kugel und der Lautsprecher nötig. Dabei gilt es einen Kompromiss zwischen kompakten Maßen und der oberen und unteren Grenzfrequenz zu finden, räumliches Aliasing zu vermeiden und durch geschickte Filterung einen möglichst großen Dynamikumfang zu erreichen.

Zu Beginn der Arbeit steht der Entwurf und Aufbau des Kugellautsprechers inklusive Verstärkung, Verkabelung und Befestigung. Um im Voraus die Abstrahleigenschaften des Arrays abschätzen zu können, werden Simulationen basierend auf dem sog. Kugelkappenmodell durchgeführt, welches die Positionen der Lautsprechermembranen auf der Kugeloberfläche modelliert. Abschließend erfolgen akustische Messungen am fertigen Prototyp des Kugellautsprechers, um damit die Abstrahlungswirkung aller Lautsprecher und ihrer gegenseitigen Beeinflussung im Gesamtsystem zu eruieren. Zur Ansteuerung wird mit diesen Daten ein geeigneter Algorithmus hergeleitet. Er beinhaltet anguläre und radiale Filter. Da letztere sehr große Bassüberhöhungen verwenden, wird eine geeignete Filterbank zur Begrenzung entwickelt.

Pledge of Integrity

I hereby certify that the work presented in this thesis is my own, that all work performed by others is appropriately declared and cited, and that no sources other than those listed were used.

Place: _____

Date: _____

Signature: _____

Eidesstattliche Erklärung

Ich versichere ehrenwörtlich, dass ich diese Arbeit selbständig verfasst habe, dass sämtliche Arbeiten von Anderen entsprechend gekennzeichnet und mit Quellenangaben versehen sind, und dass ich keine anderen als die angegebenen Quellen benutzt habe.

Ort: _____

Datum: _____

Unterschrift: _____

Danksagung

Ich möchte mich an dieser Stelle bei allen bedanken, die mich im Laufe meines Studiums begleitet und unterstützt haben. Allen voran meinen Eltern, die stets an mich glauben und mich unterstützen und mir so das Studium in dieser Intensität ermöglicht haben. Vielen Dank auch an Mona für die Kraft und Liebe, die sie mir gibt.

Besonderer Dank geht an Franz Zotter für seine herausragend gute Betreuung. Vor allem seine Begeisterungsfähigkeit, sein Fachwissen und sein Sinn für Humor waren für mich im Laufe der Arbeit stets eine Quelle von Motivation und Inspiration.

Weiters möchte ich allen Mitarbeitern und Mitarbeiterinnen am IEM danken, vor allem Brigitte Bergner und Professor Höldrich. Vielen Dank auch an die Jungs im ersten Stock für ihre Unterstützung und natürlich für die Kebap- und Schokoschneckenzeit...

Herzlichen Dank an Hermann Deutscher für den Bau des Lautsprechergehäuses und an Winfried Ritsch für die Hilfe bei der Montage.

Contents

Chapter 1

Introduction

Most musical instruments radiate their sound in a highly complex way. This means that not all frequencies are emitted into the room omnidirectionally or in the same direction. Rather they produce quite complex radiation patterns. Recording an instrument with only one or a few microphones and reproducing its sound with a stereo system cannot fully reconstruct the acoustic situation, as the recording-reproduction-system only represents a small part of the entity of the radiated sound. Therefore, recent research investigates new ways of recording and reproduction. One scientific approach, that tries to handle this task, employs spherical arrays of microphones and loudspeakers. Recording an instrument in the middle of a spherical arrangement of microphones and the reproduction of this recording with a spherical loudspeaker array could lead to a more accurate acoustical representation of the instrument. This work deals with a new method of constructing such a spherical reproduction system.

However, a more natural reproduction of instrumental sound is not the only purpose of spherical loudspeaker arrays. Moreover, musical and artistic performances in electronic music can benefit from this interesting form of sound reproduction. Another field of application is room acoustics. In general, spherical loudspeaker arrays can produce a sound beam in a variable, adjustable direction. Therefore, they can excite a room in a specified direction and be used to obtain directional room impulse responses.

The investigation of spherical arrays is fairly young and there are not many, but some pioneering works on the subject. E.g., the work of Kassakian and Wessel [KW04] mainly regards the error bounds of approximated patterns for different array designs. Some other publications concerning spherical beamforming have been published in the meantime. Zotter and Noisternig in [ZN07] present a method for dividing the beamforming algorithm into an angular and a radial part. In his diploma thesis [Pom08], Pomberger derives and implements such a two-step control system. An analytic model based on the so-called sphere cap model of spherical arrays is given in [ZSH07]. There, one also can find error bounds for the radiation error of different arrays based on the Platonic solids and in dependence of the distance to the array. The extended model in the subsequent work [ZH07] also considers the interior and exterior acoustical forces on the membranes and an electro-acoustic description. Pollow's Master thesis [Pol07] concerns theoretical and practical issues of a dodecahedral array. The most detailed work on the topic until now seems to be the PhD thesis of Zotter [Zot09]. It has a clear theoretical focus and observes many questions related to spherical sound-radiation comprehensively. Recently, Hohl constructed a microphone array, that consists of 64 microphones lying on the surface of a sphere. In [Hoh09] he describes, how this array can be used to measure radiation patterns of musical instruments.

Preview of the thesis:

Chapter 2 deals with some important theoretical basics that are necessary for the understanding of spherical beamforming. A starting point is the solution of the wave equation in spherical coordinates. This chapter introduces important terms like spherical harmonics, spherical harmonics transform, spherical harmonics analysis and synthesis and spatial aliasing.

Chapter 3 shows possibilities of constructing a spherical loudspeaker array, in particular a new design with 16 loudspeakers. This chapter also investigates the geometrical properties of the array.

Chapter 4 presents a simulation of the sound radiation of the array. To pre-estimate the capacity of the array in terms of sound reproduction, the radiation of some particular kinds of sound fields for testing will be simulated.

Chapter 5 is dedicated to the implementation of a control system to control a real array. This control system contains filters that require inaccessibly high bass boosts. Therefore, this chapter provides a way of limiting and stabilizing these filters using a dedicated type of filterbank, while maintaining a constant frequency response in the beam direction.

The control system requires a description of the transfer properties of the array. **Chapter 6** shows, how this system identification can be measured with a Laser Doppler Vibrometer. Finally, the results will be categorized according to the geometrical properties found in chapter 3.

Chapter 7 points out conclusions that can be made based on the presented results of the thesis and gives some outlook to future tasks in spherical array processing.

Chapter 2

Theory

2.1 Solution of the Wave Equation in Spherical Coordinates

The wave equation describes the temporal and spatial expansion of a wave. It is the basis of all following theoretical considerations (cf.[Wil99], [GW03], [Zot09], [TM07]). The linear lossless wave equation is a partial differential equation of the second kind, which contains the second derivatives of the sound pressure with respect to the time and the directions of propagation [TM07]. Its structure implies that a wave is the spatial propagation of an oscillation

$$\nabla^2 p = \frac{1}{c^2} \frac{\partial^2 p}{\partial t^2}. \tag{2.1}$$

Thereby the operator ∇^2 contains all second derivatives with respect to the cartesian coordinates x, y, z. In order to obtain a suitable mathematical description for spherical problems, the cartesian coordinates are transformed to spherical coordinates according to the following equations [Wil99]:

$$
\begin{aligned}
r &= \sqrt{x^2 + y^2 + z^2}, \\
\varphi &= atan2(\frac{y}{x}), \\
\theta &= -atan2(\frac{\sqrt{x^2 + y^2}}{z}).
\end{aligned}
\tag{2.2}
$$

Atan2 denotes the used MATLAB-function returning an angle between $-\pi$ and π. Mostly, φ is called azimuth and θ is called zenith. The transfomation from spherical back to cartesian coordinates can be performed by using:

$$
\begin{aligned}
x &= r \cdot \sin\theta \cdot \cos\varphi, \\
y &= r \cdot \sin\theta \cdot \sin\varphi, \\
z &= r \cdot \cos\theta.
\end{aligned}
\tag{2.3}
$$

The complete wave equation in spherical coordinates is:

$$
\frac{1}{r^2}\frac{\partial}{\partial r}(r^2\frac{\partial p}{\partial r}) + \frac{1}{r^2\sin\theta}\frac{\partial}{\partial\theta}\sin\theta\frac{\partial p}{\partial\theta} + \frac{1}{r^2\sin^2\theta}\frac{\partial^2 p}{\partial\varphi^2} - \frac{1}{c^2}\frac{\partial^2 p}{\partial t^2} = 0.
\tag{2.4}
$$

A product ansatz for seperation of variables

$$
p(r,\theta,\varphi,t) = R(r)\Theta(\theta)\Phi(\varphi)T(t)
\tag{2.5}
$$

yields four ordinary differential equation as general solution [Wil99]:

$$
\frac{d^2\Phi}{d\varphi^2} + m^2\Phi = 0,
\tag{2.6}
$$

$$
\frac{1}{\sin\theta}\frac{d}{d\theta}(\sin\theta\frac{d\Theta}{d\theta}) + [n(n+1) - \frac{m^2}{\sin^2\theta}]\Theta = 0,
\tag{2.7}
$$

$$
\frac{1}{r^2}\frac{d}{dr}(r^2\frac{dR}{dr}) + k^2R - \frac{n(n+1)}{r^2}R = 0,
\tag{2.8}
$$

$$
\frac{1}{c^2}\frac{d^2T}{dt^2} + k^2T = 0.
\tag{2.9}
$$

The four solutions. These functions must be individually solved. The first two solutions describe the angular, the third one the radial and the last one the temporal dependency of the sound field. The temporal term is not observed closer. Nevertheless, the considered physical relations are assumed to be causual.

2.1.1 Angular Term

Legendre-functions. To solve the equations (2.6) and (2.7) the associated Legendre-functions are necesary. These are well-defined functions, which can be found in literature (e.g. [Wil99]). Combining the two angular solutions leads to a set of new functions, the so called spherical harmonics (SH). They are defined as:

$$Y_n^m(\theta, \varphi) = \sqrt{\frac{2n+1}{4\pi} \frac{(n-m)!}{(n+m)!}} P_n^m(\cos\theta) e^{jm\varphi}. \tag{2.10}$$

P_n^m denotes the asociated Legendre-functions, n the order and m the degree. Because the spherical harmonics are orthonormal base functions, every square integrable function can be decomposed into a series of spherical harmonics coefficients, also called expansion coefficients. This basic property is used later for the spherical harmonics transform (cf. section 2.2).

Figure 2.1 depicts the first 16 real-valued spherical harmonics. It shows, that every order consists of $2n+1$ degrees. They are numbered from -n to n. Often a linear index nm is used:
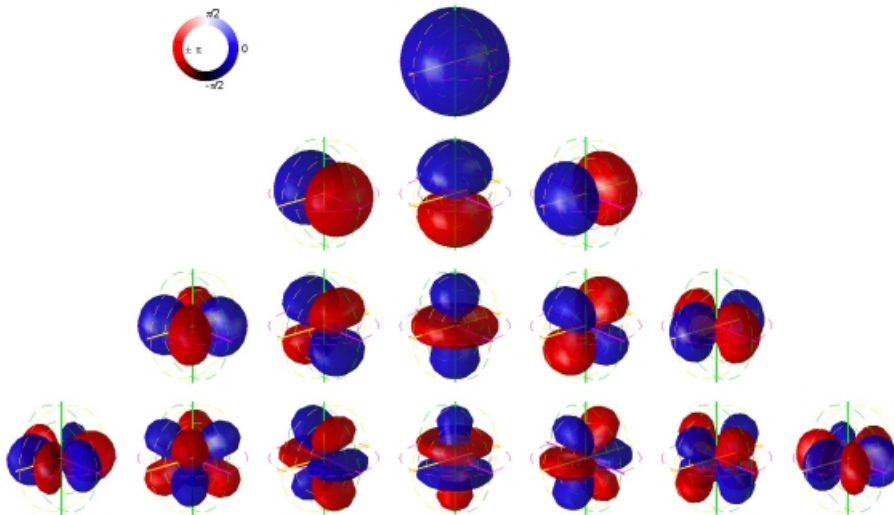
$$nm = n^2 + n + m + 1. \tag{2.11}$$

Figure 2.1: the first 16 spherical harmonics [Pom08]

2.1.2 Radial Term

Spherical Hankel-functions. For the solution of the radial term spherical Hankel- and Bessel-functions are used. The former describe incoming and the latter outgoing waves. Since an exterior problem is assumed here (cf. [Ple09]), only the spherical Hankel-function is considered. Using these functions the solution of the wave equation in the frequency domain can be determined according to Williams [Wil99] as:

$$p(r, \varphi, \theta, \omega) = \sum_{n=0}^{\infty} \sum_{m=-n}^{n} E_{nm}(\omega) h_n^{(2)}(kr) Y_n^m(\theta, \varphi), \qquad (2.12)$$

where $k = \frac{\omega}{c}$ denotes the wave number, $h_n^{(2)}$ the spherical Hankel-functions of the second kind and E_{nm} is defined by the boundary value problem (cf. chapter 5).

2.2 Spherical Harmonics Transform

As already mentioned in section 2.1.1, a function, which is defined on the sphere (for example the distribution of the sound pressure on a reference radius) can be expressed in terms of coefficients of the spherical harmonics. This is called spherical harmonics transform (SHT) [Pom08]:

$$S\{x(\theta, \varphi)\} = \chi_{nm} = \int_{S^2} x(\theta, \varphi) Y_n^{m*}(\theta, \varphi) d\theta \, d\varphi. \qquad (2.13)$$

Thereby $Y_n^{m*}(\theta, \varphi)$ denotes the complex conjugate of the spherical harmonics. The expansion coefficients are denominated with related greek letters. The index nm describes which spherical harmonic it belongs to.

The inverse spherical harmonics transform (ISHT) is:

$$S^{-1}\{\chi_{nm}\} = x(\theta, \varphi) = \sum_{n=0}^{\infty} \sum_{m=-n}^{n} \chi_{nm} Y_n^m(\theta, \varphi). \qquad (2.14)$$

Spherical Wave Spectrum. Applying the spherical harmonics transform at a certain analysis radius r_a yields the so called spherical wave spectrum [Pom08], [Wil99]:

$$\chi_{nm}(r_a) = \int_{S^2} x(r_a, \theta, \varphi) Y_n^{m*}(\theta, \varphi) d\theta \ d\varphi. \tag{2.15}$$

$\chi_{nm}(r_a)$ represents the spherical components evaluated on the analysis radius r_a. The most fundamental quantities of the sound field are the sound pressure and the sound particle velocity. Therefore two important terms can be defined:

$\psi_{nm}(r_a)$: spherical pressure spectrum

$\nu_{nm}(r_a)$: spherical particle velocity spectrum

An alternative description of the spherical harmonics transform can be found in [Pol07]. There the spherical harmonics decomposition can be seen as an inner product of the function, that should be transformed, and the related spherical harmonics:

$$\chi_{nm} = \langle x(\theta, \varphi) | Y_m^n \rangle. \tag{2.16}$$

2.3 Truncated Spherical Harmonics Transform

For an exact calculation of the transformation, theoretically an infinite number of spherical harmonics is needed, which is not realiseable. Usually only a limited subset of spherical harmonics can be controlled. For a sensible definition of such a subset it is convenient to use a truncation. Therefore equation (2.14) can be rewritten as:

$$\boxed{S^{-1}\{\chi_{nm}\} = x(\theta, \varphi) = \sum_{n=0}^{N} \sum_{m=-n}^{n} \chi_{nm} Y_n^m(\theta, \varphi).} \tag{2.17}$$

Spatial Frequency. N denotes the maximum order. A band-limited function in general does not contain high frequency components. Here a spatial frequency is meant. It describes the change rate of a function over any spatial (or angular) direction. Mathematically, this means that the decomposition of a function is truncated to the maximum order N and that any higher order coefficient vanishes [Pol07].

Sampling and Matrix Notation. Only a finite number of drivers at discrete positions on the sphere can be used. The observed spherical function is no more continuous but

discrete and a sample vector can be built containing the sample values of all the positions of the loudspeakers $\Theta_{\mathbf{k}} = (\theta_k, \varphi_k)$ with K being the number of drivers:

$$\mathbf{x} = [x(\Theta_{\mathbf{1}})\ x(\Theta_{\mathbf{2}})\dots x(\Theta_{\mathbf{K}})]^T.$$ (2.18)

The spherical harmonics are evaluated at the driver-positions. Pomberger expresses this with a compact matrix notation [Pom08]. First let us consider the values of all spherical harmonics up to the order N evaluated for one driver position and combine them to a vector:

$$\mathbf{c_N^{(k)}} = \text{vec}_N\{Y_n^m(\Theta_{\mathbf{k}})\} = \begin{bmatrix} Y_0^0(\Theta_{\mathbf{k}}) \\ Y_1^{-1}(\Theta_{\mathbf{k}}) \\ \vdots \\ Y_n^{-n}(\Theta_{\mathbf{k}}) \\ \vdots \\ Y_n^n(\Theta_{\mathbf{k}}) \\ \vdots \\ Y_N^N(\Theta_{\mathbf{k}}) \end{bmatrix}.$$ (2.19)

This leads to a Matrix $\mathbf{C_N}$ of the size $[K \times (N+1)^2]$ containing the $(N+1)^2$ spherical harmonics at the K driver locations:

$$\mathbf{C_N} = \begin{bmatrix} \mathbf{c_N^{(1)T}} \\ \mathbf{c_N^{(2)T}} \\ \vdots \\ \mathbf{c_N^{(K)T}} \end{bmatrix}.$$ (2.20)

With

$$\boldsymbol{\chi} = \text{vec}\{\chi_{nm}\},$$ (2.21)

which combines all coefficients of the $(N+1)^2$ spherical harmonics, equation (2.17) can be rewritten as:

$$\boxed{\mathbf{x} = \mathbf{C_N} \cdot \boldsymbol{\chi}.}$$ (2.22)

The decomposition of $\mathbf{x}$ in terms of spherical harmonics coefficients requires system inversion of $\mathbf{C_N}$:

$$\boxed{\boldsymbol{\chi} = \mathbf{C_N}^{-1} \cdot \mathbf{x}.}$$ (2.23)

Solvability. Depending on the form of $\mathbf{C_N}$ (often called coder matrix) this system of equations shows different behavior [Pom08]:

1. $K < (N+1)^2$: system is underdetermined, an infinite amount of solutions may exist if $(\mathbf{C_N C_N^T})^{-1}$ exists

2. $K = (N+1)^2$: exact solution exists if $\mathbf{C_N}^{-1}$ exists

3. $K > (N+1)^2$: system is overdetermined, no exact solution exists, but an aproximation can be calculated with the pseudo-inverse if $(\mathbf{C_N C_N^T})^{-1}$ exists

2.4   Analysis And Synthesis

SH-analysis (holography) of given sound pressure distributions means the evaluation of the recording of the concerned sound field with a spherical microphone array. E.g. in [Hoh09] Hohl describes the construction of a spherical microphone array with 64 microphones for the recording of musical instruments. In this experimental setup, a musician sits in the middle of the spherical construction and is surrounded by microphones. In [Ple09], Plessas points out ways of constructing a compact spherical microphone array. Here the situation is reversed: the array is surrounded by musicians. Figure 2.2 shows a block diagram for spherical harmonics decomposition of spherical microphone array data:
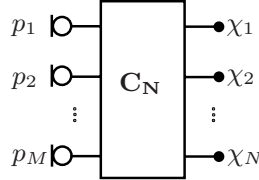
Figure 2.2: basic sound field analysis

The input of the system are the M microphone signals $\mathbf{p} = [p_1 \; p_2 \; ... \; p_M]^T$, $\mathbf{C_N}$ describes the geometrical arrangement of the microphones in terms of spherical harmonics and $\boldsymbol{\chi} = [\chi_1 \; \chi_2 \; ... \; \chi_N]^T$ are the unknown expansion coefficients:

$$\mathbf{p} = \mathbf{C_N} \cdot \boldsymbol{\chi} \Rightarrow \boldsymbol{\chi} = \mathbf{C_N^{-1}} \cdot \mathbf{p}. \tag{2.24}$$

This equation was already derived in section 2.3. Equation (2.24) and (2.23) respectively can only have an exact solution if $M = (N+1)^2$. When $M > (N+1)^2$ an approxi-

mation can be calculated using the minimization of the square error (least squares):

$$\mathbf{e} = \mathbf{p} - \mathbf{C_N} \cdot \boldsymbol{\chi},$$

$$\Rightarrow ||\mathbf{e}||^2 = ||\mathbf{p} - \mathbf{C_N} \cdot \boldsymbol{\chi}||^2 \rightarrow min. \tag{2.25}$$

SH-synthesis (holophony) regards the reproduction of a desired sound field given in its SH expansion coefficients $\boldsymbol{\chi} = [\chi_1 \ \chi_2 \ ... \ \chi_N]^T$. The desired quantity is the loudspeaker signal vector $\mathbf{l} = [l_1 \ l_2 \ ... \ l_L]^T$ containing the L loudspeaker signals. Again, a SH-matrix $\mathbf{C_N}$ describes the geometrical arrangement. Figure 2.3 depicts the principle of SH-synthesis:
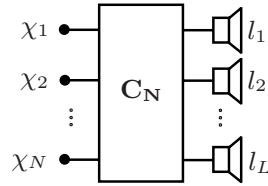
Figure 2.3: basic sound field synthesis

The discrete points for synthesis are expressed by their SH coefficients $\mathbf{C_N}^T$ that are linearly combined by the signals $\boldsymbol{l}$ to one single spherical harmonics expansion $\boldsymbol{\chi}$:

$$\boldsymbol{\chi} = \mathbf{C_N^T} \cdot \mathbf{l}. \tag{2.26}$$

A matrix inversion must be performed to obtain the required signals $\mathbf{l}$:

$$\mathbf{l} = (\mathbf{C_N^T})^{-1} \cdot \boldsymbol{\chi}. \tag{2.27}$$

Equation (2.27) must not be confused with equation (2.24). By contrast, equation (2.27) tends to have an exact solution, if $L \geq (N+1)^2$. Nevertheless, the solution is only unique, if $L = (N+1)^2$. If $L > (N+1)^2$ there is an infinite number of solutions and a minimization problem can be specified to obtain a unique solution. For example, the squared loudspeaker signals could be minimized:

$$||\mathbf{l}||^2 \rightarrow min, \tag{2.28}$$

under the constraint:

$$\boldsymbol{\chi} \overset{!}{=} \mathbf{C_N^T} \cdot \mathbf{l}. \tag{2.29}$$

17

2.5 Spatial Aliasing

When a non band-limited signal is sampled with a finite number of sample-points, aliasing occurs. Functions become ambiguous, as identical sample values may be produced by other functions as well. In this case we encounter a spatial misinterpretation, i.e. spatial aliasing. To avoid spatial aliasing and other forms of linear dependency some conditions must be fulfilled. The most important ones are [Pom08]:

1. $K \geq (N+1)^2$: There must be at least as many drivers as spherical harmonics that shall be controlled.

2. $\kappa(\mathbf{C_N}) << \infty$: The condition number [1] κ of $\mathbf{C_N}$ should be as close to 1 as possible.

In other words the postitioning of the drivers must be as good as possible according to these conditions (cf. section 3.1).

According to [ZN07], another criterion to avoid spatial aliasing concerning spherical beamformers can be given. Zotter and Noisternig give a minimal distance r_p for the projection or target radius to the surface of the sphere being about twice the radius r_0 of the array:

$$r_p \geq 2r_0. \tag{2.30}$$

They also give an upper cut-off frequency:

$$f_o \approx \frac{c}{2 \cdot r_0}. \tag{2.31}$$

---

[1] The condition number (cf. [LW]) is the ratio between the biggest and smallest singular value of a matrix. It determines the invertibility of a matrix. The closer κ is to one the more exact the matrix can be inverted.

Chapter 3

The Loudspeaker Array

Originally this thesis was dedicated to designing and constructing an icosahedral loud-speaker array for high-frequency range. As seen in the previous section 2.4 it is sufficient to have $L = (N + 1)^2$ loudspeakers to control N spherical harmonics. The icosahedron with its 20 faces provides 4 loudspeakers more than necessary for a system of order 3.

16 instead of 20 drivers. Hence, a new approach using only 16 instead of 20 drivers has been chosen. In terms of hardware effort an icosahedral system brings virtually no advantages, and to control the next higher system-order, at least 25 drivers would be necessary. As the system shall cover the mid- and high-frequency range, its dimensions should be as small as possible to minimize diffraction, shadowing effects and spatial aliasing (cf. equation (2.31)). A system with 25 drivers with the same loudspeaker membrane diameter would lead to a bigger cabinet and therefore a system with 16 drivers was chosen. To keep the dimensions small the spacing of the drivers should be as small as possible, too.

3.1   Source Distribution on the Sphere

The remaining question is, how to distribute these 16 drivers on the surface of a sphere. There is only one kind of bodies with an entirely regular layout: the Platonic solids [Ort09]. They consist of identical faces with all of the center points being equidistant to their neighbors [1]. There are only Platonic solids consisting of 4, 6, 8, 12 or 20 faces. Another group of regular solids are the Archimedian bodies. In contrast to the Platonic solids they consist of more than one kind of faces. However, there is no Archimedian body with 16 faces either.

---

[1]Meaning here all the drivers having the same distance.

Hyperinterpolation. Another way of distributing the drivers on the sphere must be found. This is a rather old topic in mathematics. The interested reader is refered to [Wim92], [HS06] or [SW01]. The paper [Zot08] compares different sampling strategies, describing the so called extremal points for hyperinterpolation the most elegant choice for our purpose. It not only uses the same number of sampling nodes as used spherical harmonics making an exact inversion of $\mathbf{C_N}$ possible (cf. section 2.3), but also the aliasing error due to higher order components appears uniformly distributed. Suitably, the extremal points for hyperinterpolation calculated by Sloan and Womersley according to [SW01] are used. They are found on [Wom09]:

Nr.	X	Y	Z
1	0	0	1
2	0,8927	0	-0,4505
3	-0,1430	0,9857	-0,0880
4	-0,7321	0,5108	-0,4506
5	0,6574	-0,7483	-0,0880
6	-0,7062	0,4759	0,5240
7	-0,6067	-0,4891	0,6266
8	-0,2949	-0,9381	-0,1815
9	0,2176	-0,7483	0,6266
10	-0,5144	-0,2374	-0,8239
11	0,8515	-0,01378	0,5240
12	0,2860	-0,4891	-0,8239
13	0,1496	0,4759	-0,8666
14	-0,9673	-0,2374	-0,08801
15	0,6813	0,7266	-0,08801
16	0,2284	0,7266	0,6479

Table 3.1: Cartesian coordinates of the extremal points for hyperinterpolation on the unit sphere due to Womersley for 16 points

With the coordinates given in table 3.1 an exact solution of the analysis problem of section 2.4 is possible and for the synthesis the equations become unique.

The second condition given in section 2.5 concerns the condition number of $\mathbf{C_N}$ and therefore its invertibility. It was calculated with the MATLAB function $cond$[2] yielding:

$$\kappa(\mathbf{C_N}) = 1,55.$$

This means that $\mathbf{C_N}$ here is rather well conditioned and that the matrix inversion should go without problems. As will be seen in chapter 5, for the control system a decoder is necessary that requires system inversion. With a small condition number the entries of the decoder matrix will be bounded to rather small values, and therefore decoding only has negligible influence on the accessible dynamic range and playback SNR.

Visualization. A MATLAB-script has been written to visualize the chosen distribution of points on the sphere. There the loudspeakers are represented by simple circles rotated from the north pole to the remaining positions of table 3.1. Therefore the cartesian coordinates are transformed to spherical coordinates with equation (2.2) and then two rotation matrices were applied:

$$rotz = \begin{pmatrix} cos(\varphi) & -sin(\varphi) & 0 \\ sin(\varphi) & cos(\varphi) & 0 \\ 0 & 0 & 1 \end{pmatrix}, \tag{3.1}$$

$$roty = \begin{pmatrix} cos(\theta) & 0 & -sin(\theta) \\ 0 & 1 & 0 \\ sin(\theta) & 0 & cos(\theta) \end{pmatrix}. \tag{3.2}$$

Note, that the center positions of the loudspeakers do not lie on the surface of the sphere. Rather they must be plunged into the construction. The distance of the loudspeaker center to the center of the sphere is denominated with r_M and depends on the radius of the loudspeaker membrane. It can be calculated according to figure 3.1

$$r_M = \sqrt{r_0^2 - r_{LS}^2}, \tag{3.3}$$

with r_0 being the radius of the sphere and r_{LS} the radius of the loudspeaker. Figure 3.2 shows the produced MATLAB-plot with $r_0 = 8,5$ cm and $r_{LS} = 3,25$ cm.

---

[2]Note that the second kind condition number is meant.
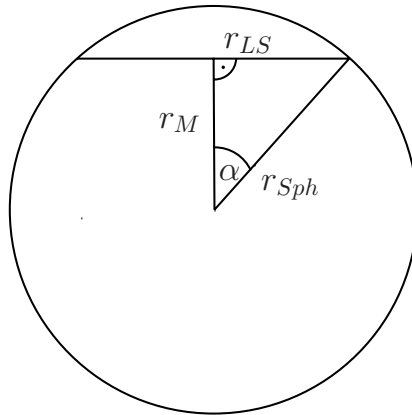
Figure 3.1: The rectangular triangle formed by r_m, r_{LS}, and r_0
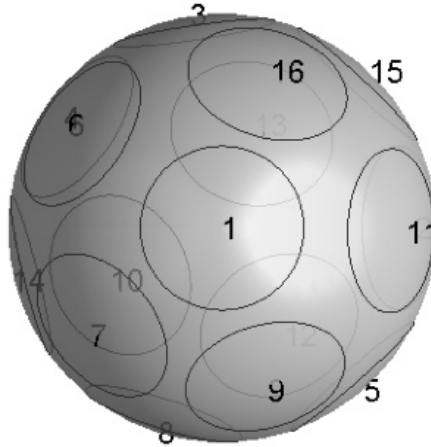
Figure 3.2: MATLAB-plot of the spherical loudspeaker array with the 16 drivers marked with circles providing a view onto the north pole

3.2 Construction of the Sphere

To give the loudspeakers a volume to operate on and to be able to connect the drivers in a comfortable way, the sphere was designed to be hollow. However, the construction of a hollow sphere is not a trivial task. Many approaches were discussed and the most important ones will be presented here. One of the most challenging experiences was to provide accurate positioning of the drivers in the final construction. As shown in [Ple09], even a slight positioning error can already produce a lot of synthesis errors.

Glass fiber reinforced plastics (GRP). GRP is a common building material. It is light and rather easy to handle. Webs of glass fiber are soaked in polyester resin and put on a negative model, which has to be built first. This makes this approach not effective for the construction of only one sphere, but would be a good choice for serial production. Furthermore, it is rather difficult to find the centers of the drivers after the construction of the sphere. Therefore the holes for the drivers should be part of the negative model already.

Plywood construction with circular rings. Another idea was to construct two hemispheres and cement them together afterwards. This could be made by cutting out circular rings with decreasing radii with a laser cutter and bonding them together. So an approximation of the sphere could be realized and the residual wood could be removed using a turnery. The radii can be calculated as shown in figure 3.3:
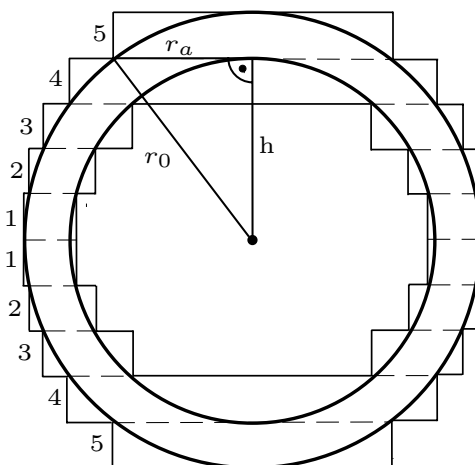
Figure 3.3: Cross-section of the approximated hollow sphere

$$r_a = \sqrt{r_0^2 - h^2}. \tag{3.4}$$

The residual inner and outer radii can be calculated using the same formula. h is determined by the ring-number times the thickness of one ring. Note, that for the inner radii the sphere is approximated from the inside and for the outer radii from the outside. Using thinner boards yields a better approximation of the sphere and less wood has to be removed.

Although this is an easy way to construct a hollow sphere, the disadvantage is that the sphere could be damaged during turning because the wood fibers could frazzle. And we have again the same problem with finding the centers for the drivers and cut the holes into the construction.

3D-Plotter. In architecture and design so called 3D-plotters are used to construct a model of future constructions to be able to estimate their shape in advance. On the basis of a 3D-CAD-model a 1 to 1 model is created in the plotter. There are several suitable materials like different kinds of plastics and metal. Here a simple 3D-model of a sphere with a suitable radius and the holes for the drivers could easily been modeled. But this attempt was not chosen in favor of the approach described in the following paragraph.

Polyhedron approach. The existing spherical array of the IEM is an icosahedron. The 20 driver are placed in the center of each face yielding its correct position. The same approach can be made here. A polyhedron is searched consisting of 16 polygons. This body can be obtained by dividing the surface in so called Voronoi-cells. Therefore, first a triangulation is applied connecting all the 16 points on the sphere with one another. The sphere is now divided into triangles and then the dual body must be found. This is done by connecting perpendicular bisectors of the sides of the triangles. The center positions of the triangles thus become the vertices of the obtained dual polyhedron. This is visualized in figure 3.4:
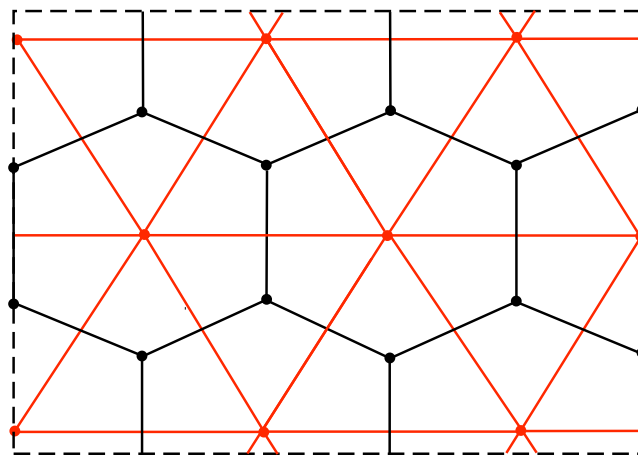
Figure 3.4: plane Voronoi tesselation: the red dots are the center-positions of the drivers, the black dots are the vertices of the polygons

On [Ren09] a little program called STRIPACK can be found that calculates the Voronoi-points for a given point distribution on the sphere. This was applied to the 16 points giving back the coordinates of the Voronoi-points on the sphere. As we wanted to start with polyhedra consisting of plane polygons, a factor was calculated to multiply the coordinates with and bring them to the same plane as the drivers.
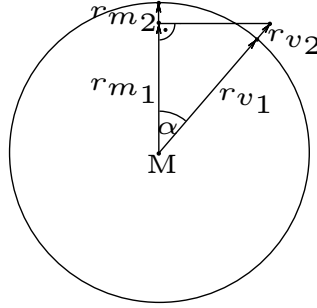
Figure 3.5: Visualization for the calculation of the voronoi points: the vector r_{v_1} must be stretched to r_{v_2}

The angle α can be calculated with the inner product of the vectors r_{m_2} and r_{v_1}:

$$\cos\alpha = \frac{\langle \vec{r}_{m_2}, \vec{r}_{v_1}\rangle}{||\vec{r}_{m_2}|| \cdot ||\vec{r}_{v_1}||} = \frac{\vec{r}_{m_2}^T \cdot \vec{r}_{v_1}}{r_0^2}, \tag{3.5}$$

as $||\vec{r}_{m_2}|| = ||\vec{r}_{v_1}|| = r_0$. Due to the Pythagorean Theorem $cos\alpha$ can also be written as

$$\cos\alpha = \frac{r_{m_1}}{r_{v_2}}. \tag{3.6}$$

By putting (3.5) in (3.6) and with $r_{m_1} = r_M$ the wanted segment $r_V := r_{v_2}$ can finally be calculated:

$$r_V = r_M \cdot \frac{r_0}{\vec{r}_{m_2}^T \cdot \vec{r}_{v_1}}. \tag{3.7}$$

This was done for all points yielding the polyhedron shown in figure 3.6.
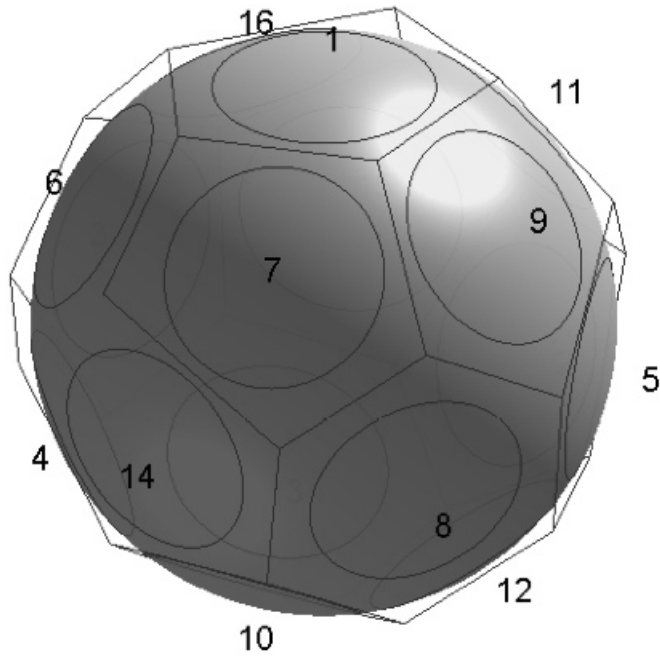
Figure 3.6: MATLAB-plot of the plane Voronoi-decomposition of the surface of the spherical loudspeaker array

The MATLAB-coordinates were imported in Rhino3D, a 3D-CAD-program. There a 3D-model of the polyhedron was created. This was done segment by segment. One is depicted in figure 3.7 assuming a wall thickness of 16 mm.
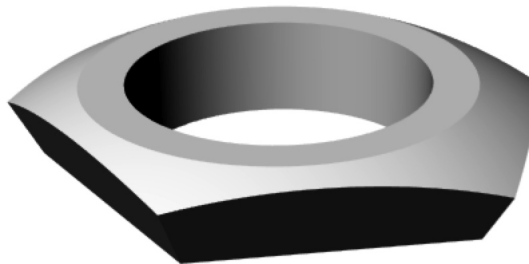
Figure 3.7: one segment of the modeled sphere

Combining all 16 segments yields the complete polyhedron. It is no more a plane solid, but the vertices are rounded. This way no more turning is necessary and the body has its original round form.
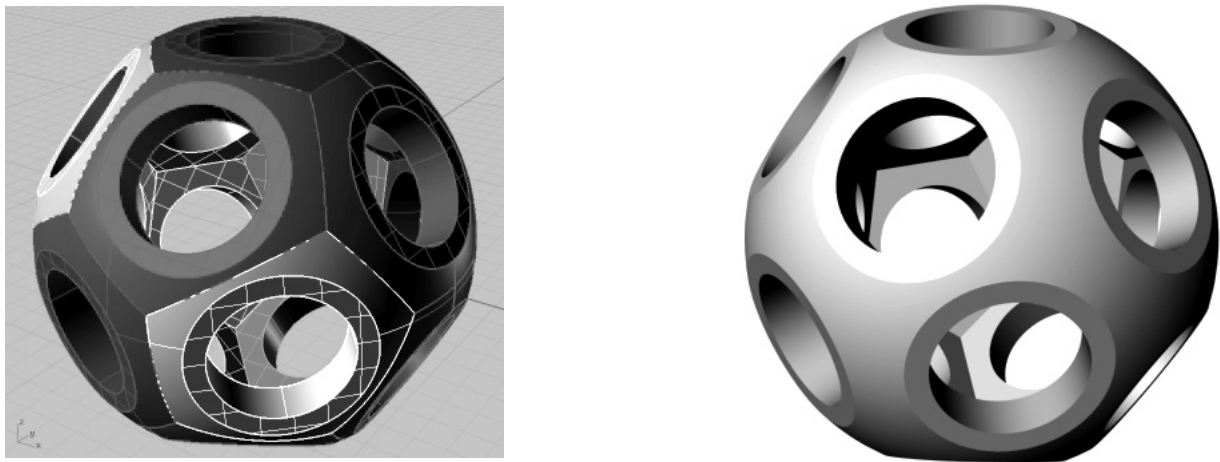
Figure 3.8: The Rhino-3D-Model: on the left consisting of the single elements, on the right the rendered version

Construction with CNC-machine. The segments were produced using a CNC-machine (CNC = computerized numeric control). Therefore all of the segments were brought to the x-y-plain and milled out of an MDF-board (MDF = medium density fiber). The result is shown in figure 3.9. Normal wood has different vibration behavior in and off the fiber-direction yielding different resonance-behavior. This is not wanted as the resonances should be as little as possible or at least homogeneous. MDF has the advantage of being a very homogeneous material [3]. Furthermore it is cheap and its handling is rather comfortable making it a very commonly used material in the construction of loudspeaker cabinets. After the CNC-machine the segments were then bonded together in the right order and finished in black. All these workings were done by *Hermann Deutscher*, a carpenter located near Graz.

Choosing the drivers. The chosen Peerless 830983 extended frequency range drivers have a membrane diameter of 2 inches. Their maximum long-term power is indicated with 60W. The Thiele-Small-Parameters and the frequency response can be found in the appendix A.

---

[3]Here I would like to thank *Thomas Andrä* and *Peter Mörth* for the helpful discussions.

Figure 3.9: left: The milled MDF board with the segments after the CNC-machine; right: The finished cabinet

3.3 Geometrical Properties

It can be seen that the polyhedron does not have an entirely irregular form, as supposed. Rather it shows certain kinds of symmetry and repetition. It is constructed of 12 pentagons and 4 hexagons. As pointed out by the carpenter, "*there is only one kind of pentagon and one kind of hexagon*". Furthermore, the center positions of the hexagons lie on the vertices of a tetrahedron. Using the rotation matrices of equations (3.1) and (3.2) the coordinates given in table 3.1 can be transformed, so that one hexagon comes to lie on the north pole. The transformed coordinates are given in table 3.2 and figure 3.10 depicts the new arrangement of loudspeakers in the Voronoi-model. Also the drivers are given a new numbering according to a spiral shaped sequence.

Table 3.2 and figure 3.10 show the nearly perfect symmetry of the polyhedron. The drivers are arranged in three rings. The first one consists of six loudspeakers (numbers 2 to 7) with the same zenith angle, the second one also contains six speakers (numbers 8 to 13), but with an alternating zenith angle and the third one has three drivers (numbers 14 to 16) again with a constant zenith. The 8th loudspeaker was chosen to be the front speaker, meaning it lies on the positive x-axis. Due to the regular arrangement of the hexagons on the vertices of a tetrahedron, each of them can be chosen as north pole without changing the geometrical properties.

Nr.	X	Y	Z	Azimuth	Zenith
1	0.0000	-0.0000	1.0000	-82.9801	-0.0020
2	0.7302	-0.4383	0.5241	-30.9735	-58.3951
3	-0.0000	-0.8517	0.5240	-90.0000	-58.3959
4	-0.7447	-0.4133	0.5241	-150.9714	-58.3946
5	-0.7376	0.4258	0.5241	150.0008	-58.3927
6	0.0145	0.8515	0.5241	89.0273	-58.3920
7	0.7376	0.4258	0.5241	29.9987	-58.3932
8	0.9834	-0.0083	-0.1815	-0.4860	-100.4577
9	0.4645	-0.8205	-0.3334	-60.4861	-109.4730
10	-0.4989	-0.8474	-0.1815	-120.4866	-100.4590
11	-0.9428	0.0080	-0.3333	179.5130	-109.4710
12	-0.4844	0.8558	-0.1815	119.5135	-100.4557
13	0.4783	0.8125	-0.3333	59.5141	-109.4697
14	0.4989	-0.0042	-0.8666	-0.4830	-150.0716
15	-0.2531	-0.4299	-0.8667	-120.4884	-150.0729
16	-0.2458	0.4342	-0.8666	119.5124	-150.0695

Table 3.2: Cartesian and spherical coordinates for the 16 points after transformation of coordinates and reordering
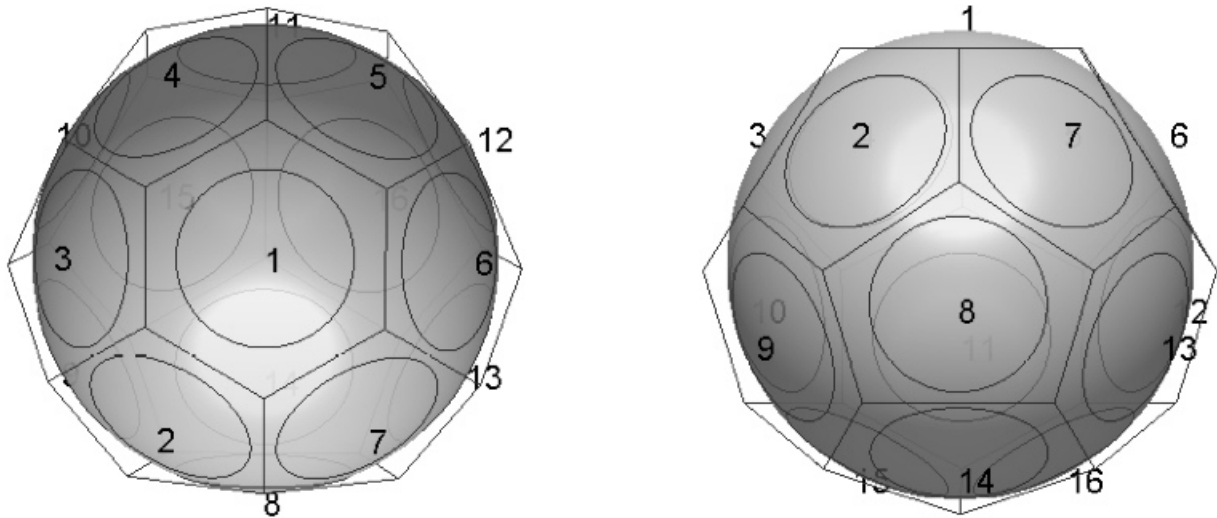
Figure 3.10: The Voronoi-model after the transformation: on the left seen from above, on the right seen frontally

Final mounting. The final mounting of the loudspeaker array was accomplished regarding the above information. The support was installed at the south pole, which is exactly the vertex of the three pentagons, formed by the third ring of loudspeakers. For amplification two 8-channel Bittner amps are used. They are connected with the array using a 20-channel multicore cable with a MIL-C connector. The outlet of the cables at the sphere is installed on the opposite side of the 8th loudspeaker. This way front and back of the array become clear also visually.

Figure 3.11: The final loudspeaker array: on the left seen frontally, on the right seen from the side

Chapter 4

Array Simulation

4.1 Spherical Cap Model

Based on the papers [ZSH07] and [ZH07] a simulation of the radiation of the array was written in MATLAB. Due to these works an analytic model of the spherical array can be found, using a model of the boundary condition for the radial sound particle velocity $v(\varphi, \theta)\big|_{r_0}$ on the surface of the sphere with radius r_0, called spherical cap model. This distribution can be decomposed into L regions, each one meaning the area of a loudspeaker membrane with its individual particle velocity v_l [ZSH07]:

$$v(\varphi, \theta)\big|_{r_0} = \sum_{l=1}^{L} v_l \cdot a_l(\varphi, \theta)). \tag{4.1}$$

Aperture function. a_l is called aperture function. Its value can be 1 or 0 and they do not overlap. It describes the part of the array, where sound waves leave the array, meaning the area of the drivers. Therefore, it can be written as:

$$a_l(\varphi, \theta) = \begin{cases} 1 & \text{at } l^{th} \text{ loudspeaker,} \\ 0 & \text{otherwise.} \end{cases} \tag{4.2}$$

In other words, the areas, where $a_l = 0$ describe the solid part of the array, i.e. $v = 0$. First let us consider the aperture function of one loudspeaker, most suitably the one located at the north pole.

In the spherical harmonics domain a compact expression for the calculation of the aperture function exists and therefore from this moment on all calculations of this subsection are done in the spherical harmonics domain [1]. In [ZH07] an equation for the calculation of the l-th aperture function belonging to the l-th loudspeaker is given:

$$A_{nm}^{(l)} = SHT\{a^{(l)}(\varphi, \theta)\} = Y_{nm}^*(\varphi_l, \theta_l) \cdot 2\pi N_{nm} \int_{\cos(\frac{\alpha}{2})}^{1} P_n[\cos(\theta)] \cdot d(\cos(\theta)), \qquad (4.3)$$

where N_{nm} are normalization constants, $P_n(x)$ are the Legendre polynomials and α is the opening angle of one driver. For its calculation let us take a look back to figure 3.1. According to trigonometry $\sin(\alpha)$ can be calculated due to:

$$\sin(\alpha) = \frac{r_{LS}}{r_{Sph}} = \frac{2,5 \text{ cm}}{8,5 \text{ cm}} \approx 0,2899, \qquad (4.4)$$

yielding an opening angle of:

$$\alpha = 2 \cdot \arcsin(\sin(\alpha)) \approx 0,5882 \approx 33,7°. \qquad (4.5)$$

When calculating the aperture function coefficients for the north pole cap the azimuthal dependence of φ can be omitted. This polar cap model $\hat{A}_n$ is now brought to the remaining positions by spherical convolution of a_l [ZSH07] for the north pole with the Dirac distribution in the spatial domain yielding a multiplication with the corresponding conjugate spherical harmonics $Y_{nm}^*(\varphi_l, \theta_l)$ in the spherical harmonics domain due to:

$$\delta(\varphi - \varphi_l) \cdot \delta(\theta - \theta_l) \xleftarrow{SHT} Y_{nm}^*(\varphi_l, \theta_l). \qquad (4.6)$$

In the spherical harmonics domain equation (4.1) can be rewritten as [2]:

$$\nu_{nm}\big|_{r_0} = \sum_{l=1}^{L} v_l \cdot \hat{A}_n \cdot Y_{nm}^*(\varphi_l, \theta_l). \qquad (4.7)$$

---

[1] Only for the final calculation of the sound pressure the inverse transform is performed to be able to plot the gained sound pressure distribution.

[2] Note that the conjugate can be omitted due to the usage of real valued spherical harmonics.

Setting all the driver velocities to 1 yields the expansion coefficients of the entire spherical cap model:

$$A_{nm} = \sum_{l=1}^{L} \hat{A}_n \cdot Y_{nm}^*(\varphi_l, \theta_l). \tag{4.8}$$

This formula was used to plot the spherical cap model (cf. figures 4.1 and 4.2). There exists an alternative way of calculating the expansion coefficients of the spherical cap model. This is shown in [ZH07]. The coefficients calculated according to equation (4.3) can be written in an $(N+1)^2$ element vector $\vec{A}^{(l)}$:

$$\vec{A}^{(l)} = \mathbf{vec}\{A_{nm}^{(l)}\} = \begin{bmatrix} A_{0,0}^{(l)} \\ A_{1,-1}^{(l)} \\ \vdots \\ A_{n,-n}^{(l)} \\ \vdots \\ A_{n,n}^{(l)} \\ \vdots \\ A_{N,N}^{(l)} \end{bmatrix}. \tag{4.9}$$

In a next step all these coefficient vectors for all the L caps can be gathered in one single matrix $\mathbf{A}$ which will be important in the next step when calculating the velocities of the drivers:

$$\mathbf{A} = \left[\vec{A}^{(1)}, ..., \vec{A}^{(L)}. \right] \tag{4.10}$$

Simulation of the spherical cap model. The performed simulation calculates the SH-coefficients for the spherical cap model according to equation (4.8). Therefore the spherical harmonics must be evaluated at all the driver positions (φ_l, θ_l). This was done for several point distributions according to [Wom09] and for different maximum orders $nmax$. To gain reasonable values for the plots, an inverse SH-transform according to equation (2.17) must be performed. Therefore the spherical harmonics must be evaluated for a set of equidistant points on the sphere (here 10201). Furthermore, one has to take care of using practical opening angles according to equation (4.4). Note, that for all plots in figures 4.1 and 4.2

$$v^{(l)} = 1, \forall l. \tag{4.11}$$
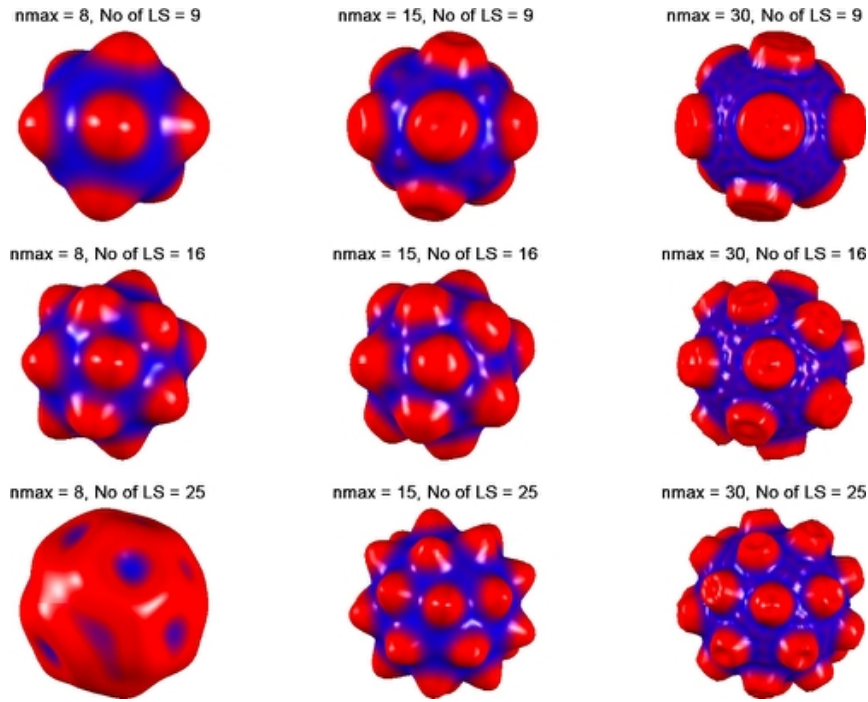
Figure 4.1: Cap model for 9, 16 and 25 drivers with different values of $nmax$
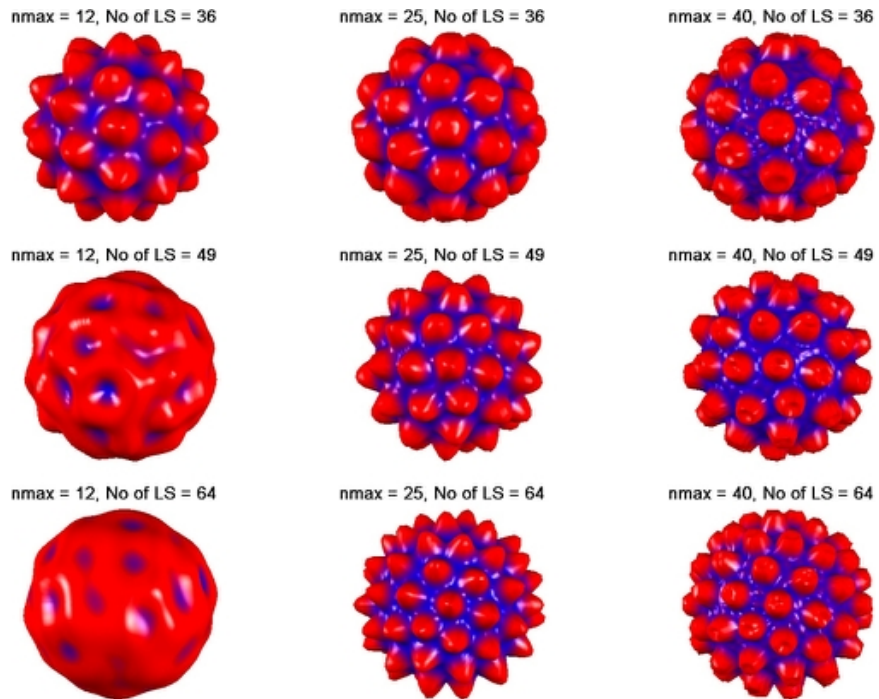
Figure 4.2: Cap model for 36, 49 and 64 drivers with different values of $nmax$

The above plots show the influence of the maximum order $nmax$ and the number of drivers. Variation of $nmax$ is only important here to gain different displays. In reality $nmax \to \infty$ and therefore $nmax$ should be as big as possible for all further simulations to obtain a cap model with a realistic and reasonable shape.

4.2   Calculation of the Driver Velocity Vector

The simulation shall demonstrate how a certain radiation pattern is reproduced by a given array. As any radiation pattern can be decomposed in a set of spherical harmonics, a first step could be to simulate, how the spherical harmonics are reproduced by the array. [Wil99] gives a formula how the expansion coefficients of such a pressure pattern at a certain distance [3] r_p $\psi_{nm}(kr_p)$ can be calculated, when the expansion coefficients of the particle velocity on the surface r_0 of the sphere $\nu_{nm}\big|_{r_0}$ as a boundary condition are given:

$$\psi_{nm}(kr_p) = i\rho_0 c \cdot \frac{h_n(kr_p)}{h_n'(kr_0)} \cdot \nu_{nm}\big|_{r_0}. \tag{4.12}$$

with $c = 343\frac{m}{s}$ the speed of sound at room temperature, $i = \sqrt{-1}$ being the imaginary unit, the wave number $k = \frac{\omega}{c}$ and $\rho_0 = 1.2$ the density of the air; h_n denominates the spherical Hankel function of the second kind, h_n' its derivative. $\nu_{nm}\big|_{r_0}$ can be obtained by a spherical harmonics transform of equation (4.1):

$$\boldsymbol{\nu}\big|_{r_0} = \sum_{l=1}^{L} \vec{A}^{(l)} \cdot v^{(l)} = \mathbf{A} \cdot \begin{bmatrix} v^{(1)} \\ v^{(2)} \\ \vdots \\ v^{(L)} \end{bmatrix} = \mathbf{A} \cdot \mathbf{v}. \tag{4.13}$$

As in equation (4.12) only the Hankel functions depending on the order n are used, a convenient notation must be found. This is done as supposed in [ZH07] with a diagonal matrix. In the diagonal stand the corresponding H_n vector elements repeated $(2n + 1)$ times. Defining

$$H_n := \frac{h_n(kr_p)}{h_n'(kr_0)}, \tag{4.14}$$

yields:

---

[3] Also called projection radius.

$$\mathbf{diag}(H_n) := \begin{bmatrix} H_0 & 0 & 0 & 0 & 0 & \dots & 0 \\ 0 & H_1 & 0 & 0 & 0 & \dots & 0 \\ 0 & 0 & H_1 & 0 & 0 & \dots & 0 \\ 0 & 0 & 0 & H_1 & 0 & \dots & 0 \\ 0 & 0 & 0 & 0 & H_2 & \dots & 0 \\ \vdots & \vdots & \vdots & \vdots & \vdots & \ddots & \vdots \\ 0 & 0 & 0 & 0 & 0 & \dots & H_N \end{bmatrix}. \tag{4.15}$$

Putting equations (4.13) and (4.15) in equation (4.12) yields a compact formula for the calculation of all the expansion coefficients of the desired spherical wave spectrum of the sound pressure:

$$\boxed{\boldsymbol{\psi}(kr_p) = i\rho_0 c \cdot \mathbf{diag}(H_n) \cdot \mathbf{A} \cdot \boldsymbol{v},} \tag{4.16}$$

with the dimensions (N: maximum order of spherical harmonics in calculations; L: number of drivers):

$$[(N+1)^2 \times 1] = [(N+1)^2 \times (N+1)^2] \cdot [(N+1)^2 \times L] \cdot [L \times 1]. \tag{4.17}$$

To obtain the required input velocity vector $\boldsymbol{v}$ for a specified choice of $\boldsymbol{\psi}(kr_p)$ a matrix inversion is required. Thus we define a new $[(N+1)^2 \times L]$ matrix $\mathbf{Q}$:

$$\mathbf{Q} := i\rho_0 c \cdot \mathbf{diag}(H_n) \cdot \mathbf{A}. \tag{4.18}$$

So $\boldsymbol{v}$ can easily be calculated as:

$$\boxed{\boldsymbol{v} = \mathbf{Q}^{-1} \cdot \boldsymbol{\psi}(kr_p)} \tag{4.19}$$

and the dimensions are:

$$[L \times 1] = [L \times (N+1)^2] \cdot [(N+1)^2 \times 1]. \tag{4.20}$$

Of course this equation can only be solved, if the inverse $\mathbf{Q}^{-1}$ exists. And if the matrix $\mathbf{Q}$ is not square, the pseudo-inverse must be used. There are two possibilities of calculating $\mathbf{Q}^{-1}$ [Pom08]:

1. Including the higher order harmonics: All the entries of $\mathbf{Q}$ are used for the inversion and the pseudo inverse must be used.

2. N_c-subspace: only the entries of $\mathbf{Q}$ which actually can be controlled are used for the inversion yielding an $[L \times L]$-matrix and exact inversion, if the inverse exists. Note, that in this case also the vector $\boldsymbol{\psi}(kr_p)$ must be truncated.

Having the correct membrane velocities for the wanted sound pressure distribution yields its simulated expansion coefficients as:

$$\hat{\boldsymbol{\psi}}(kr_p) = \mathbf{Q} \cdot \boldsymbol{v} \tag{4.21}$$

and the sound pressure is obtained by inverse spherical harmonics transform according to equation (2.22).

4.3   Radiation Simulation of Spherical Harmonics

In general $\boldsymbol{\psi}(kr_p)$ can be an arbitrary vector describing some kind of sound field. As here we want the nm-th spherical harmonic to be simulated, this $(N+1)^2$ vector only contains one entry unequal zero namely one at the nm-th position. For example, for the first spherical harmonic:

$$\boldsymbol{\psi}(kr_p) = \begin{bmatrix} 1 & 0 & 0 & \dots & 0 \end{bmatrix}^T. \tag{4.22}$$

If we suppose $\boldsymbol{\Psi}(kr_p)$ to be an identity matrix, the velocity coefficients for all controllable spherical harmonics can be calculated in one single step. Note, that if $(N+1)^2 > L$ only the first L columns of this matrix are used [4]. Finally we get an $[(N+1)^2 \times L]$ matrix $\mathbf{V}$ containing the associated velocity vectors as its columns:

$$\boldsymbol{\Psi}(kr_p) = \mathbf{Q} \cdot \mathbf{V}, \tag{4.23}$$

with the dimensions:

$$[(N+1)^2 \times L] = [(N+1)^2 \times (N+1)^2] \cdot [(N+1)^2 \times L] \cdot [L \times L]. \tag{4.24}$$

Spherical harmonics.   As already mentioned, spherical functions can be interpreted as a series of weighted spherical harmonics. To see how an arbitrary spherical function can be reproduced by a given array it is helpful to observe the radiation of the spherical harmonics by this geometry. This can be regarded as an intermediate step. The vector according to

---

[4]The remaining spherical harmonics can be simulated, too, but will lead to incorrect display, since only L spherical harmonics are controllable with L drivers.

equation (4.22) is used as an ideal coefficients vector and then put into equation (4.19) to calculate the membrane velocities of the drivers. With (4.21) the coefficients vectors of the sound field how they are reproduced by the array can be calculated and performing the inverse spherical harmonics transform yields the pressure values in dependence of azimuth and zenith, as needed for plotting. Again the inverse transform is performed as multiplication with a matrix containing the spherical harmonics evaluated at the 10201 sphere points, as described before.

Here the spherical harmonics for three important frequencies calculated using the higher order harmonics up to the order $nmax = 30$ are shown. For the remaining plots, containing more frequencies and the calculation in the truncated subspace, the reader is refered to the appendix C.

Up to 1500 Hz nearly no deviation of the spherical harmonics can be observed. At 2500 Hz spherical aliasing begins to deform the spherical harmonics and in the third plot they begin to become too inaccurate. To avoid spatial aliasing a spatial anti-aliasing filter would be necessary for band-limitation.

The first 16 SH at r $_a$=1m, f=1500Hz, nmax=30
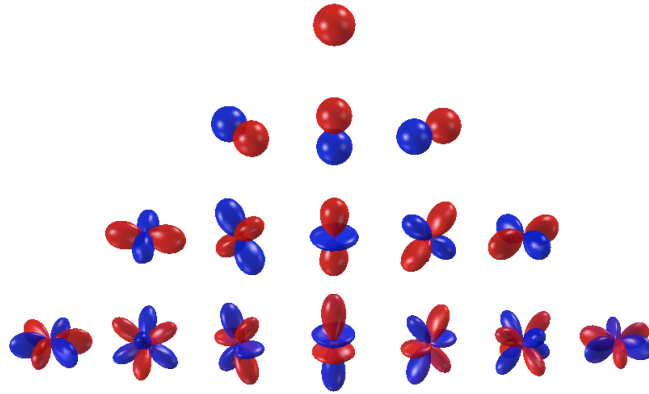
The first 16 SH at r $_a$=1m, f=2500Hz, nmax=30
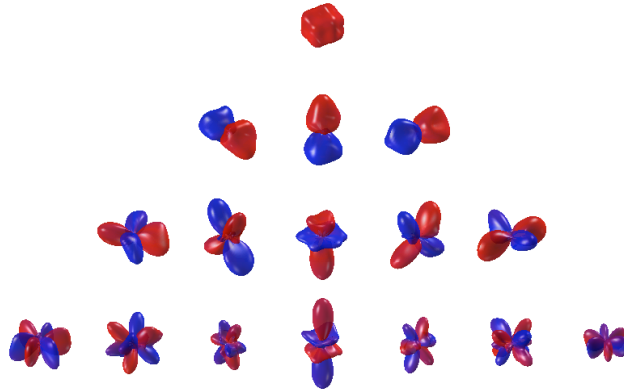
The first 16 SH at r $_a$=1m, f=3000Hz, nmax=30
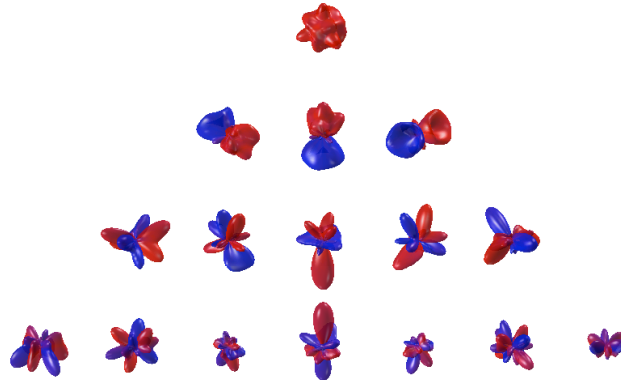
Figure 4.3: radiation of the first 16 spherical harmonics using higher order harmonics by an array with 16 drivers at a distance of 1m and at three different frequencies; the cap model was calculated using a maximum order $nmax = 30$

4.4 Forming a Beam

One of the main purposes of a spherical beamformer is to produce a sound beam in a desired direction. This beam can be regarded as a Dirac delta-distribution dependent on the angles azimuth and zenith. It can be written as:

$$\delta(\varphi - \varphi_b) \cdot \delta(\theta - \theta_b) = \begin{cases} \infty & \text{at the position } (\varphi_b, \theta_b), \\ 0 & \text{otherwise.} \end{cases} \qquad (4.25)$$

According to equation (4.6) this beam can easily be calculated as an evaluation of the spherical harmonics at the position (φ_b, θ_b) yielding the expansion coefficients for the beam:

$$\psi_{nm} = Y_n^{m*}(\varphi_b, \theta_b). \qquad (4.26)$$

Theoretically the beam would be infinitely narrow, but as the spherical harmonics order is bounded, the width of the beam depends on the maximum order. The higher the order, the more narrow the beam, but also more side lobes are produced. Of course the form of the beam also depends on the expansion term and therefore on the array geometry, the frequency and the analysis distance. With higher frequencies and less distance, more aliasing will occur.

The analytic beam. But first let us look at a so called analytic beam, a beam reproduced by the desired array, but without any errors, i.e. spatial aliasing. Figure 4.4 shows such an analytic beam pointing to the left $(\varphi_b, \theta_b) = (\frac{\pi}{2}, -\frac{\pi}{2})$. This analytic beam can only be obtained, if no higher order harmonics are included in the calculation and therefore $N = \sqrt{L} - 1$ for all calculations.
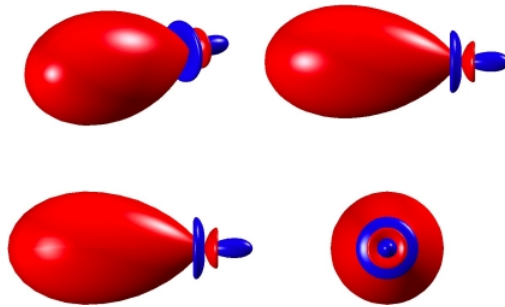
Figure 4.4: analytic beam pointing to $(\varphi_b, \theta_b) = (\frac{\pi}{2}, -\frac{\pi}{2})$ displayed in the three planes of the coordinate system for an array with 16 drivers

A real beam. Limiting $nmax$ to $\sqrt{L}-1$ is physically wrong for the calculation of the cap model. So the calculation must be performed as described in the above section. Again first the velocity coefficients are calculated with equation (4.19) using equation (4.26). Then $\boldsymbol{v}$ is inserted into (4.21) and with the inverse spherical harmonics transform the plotable sound pressure values are calculated. It is obvious, that the calculations of $\mathbf{Q}^{-1}$ again can be performed in the truncated subspace or including higher order harmonics.

For both kinds of calculation the matrix $\mathbf{Q}$ and the vector $\boldsymbol{\psi}$ are first calculated with a maximum order of $nmax = 30$. The calculation of the velocity vector $\boldsymbol{v}$ according to equation (4.19) can then be performed in the two ways: with all the entries of $\mathbf{Q}$ yielding a size of $[16 \times 961]$ for $\mathbf{Q}^{-1}$ and $[961 \times 1]$ for $\boldsymbol{\psi}$ or with the entries of the upper left $[16 \times 16]$ submatrix of $\boldsymbol{Q}$ and a truncated vector $\boldsymbol{\psi}$ with the size $[16 \times 1]$. The final calculation of the coefficient vector according to equation (4.21) yields a $[961 \times 1]$-vector in both cases.

Figures 4.5 and 4.6 depict the results for both kinds of calculation. The figures show, that for lower frequencies the truncated subspace approach seems to lead to better results, while for higher frequencies the included higher order harmonics seem to perform better. Maybe it is recommendable to use a mixture between the two options. Furthermore, the border for a reasonable aliasing cut off frequency lies somewhere between 2500 and 3000 Hz. Above this frequency, the side lobes become inacceptably huge. This bound must yet be confirmed according to listening tests. In the case of subspace calculation the beams with higher frequencies reach a far higher amplitude. This may result from the missing control of the higher order harmonics.

nmax = 30, r $_a$ = 1m, No of LS: 16

250Hz 750Hz 1500Hz

2000Hz 2500Hz 3000Hz

5000Hz 7500Hz 10000Hz
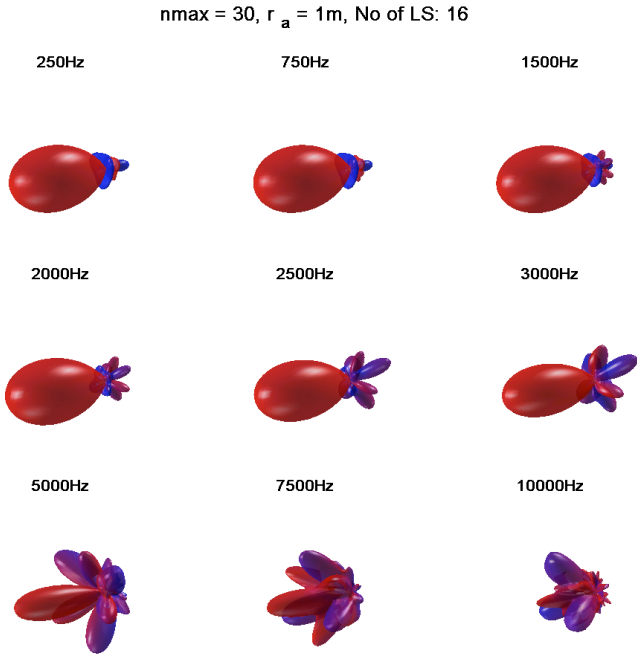
Figure 4.5: beam to the left calculated including higher order harmonics

nmax = 30, r $_a$ = 1m, No of LS: 16

250Hz 750Hz 1500Hz

2000Hz 2500Hz 3000Hz

5000Hz 7500Hz 10000Hz
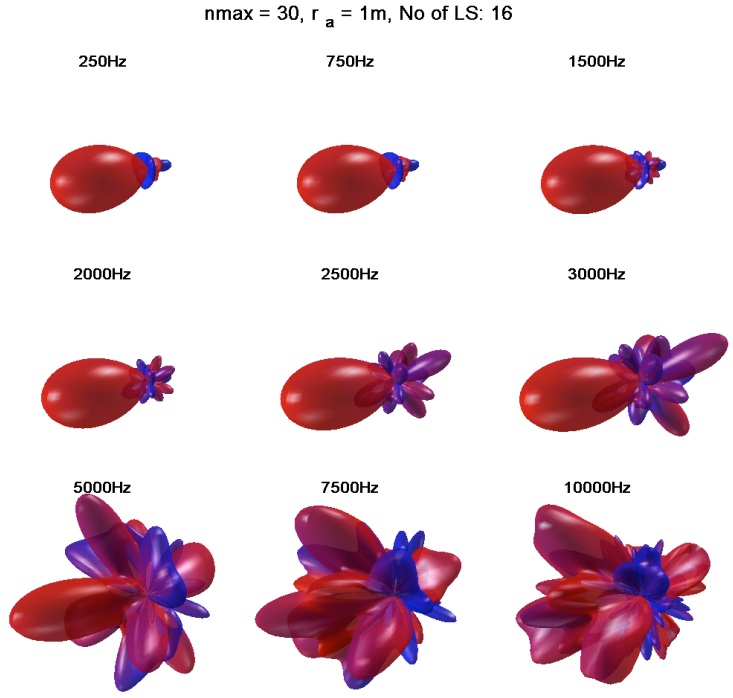
Figure 4.6: beam to the left calculated using the truncated subspace

Chapter 5

System Control

5.1 Basic Description

Gaining control over the loudspeaker system means being able to provide the drivers with suitable voltages to obtain a wanted directivity pattern (sound pressure field given e.g. by the expansion coefficients) at a certain projection radius r_p. This pattern can be defined in two different basic ways:

a) the sound particle velocity distribution on the surface of the sphere r_0: $v(\varphi, \theta)\big|_{r_0}$

b) the sound pressure distribution at the analysis radius r_a: $p(\varphi, \theta)\big|_{r_a}$

These two arrangements are shown in figure 5.1. In both cases the pattern, which is synthesized on r_a [1] is projected to r_p by a propagation term. Looking back to the solution of the wave equation in the frequency domain as given in equation (2.12) [2]

$$p(r, \varphi, \theta, \omega) = \sum_{n=0}^{\infty} \sum_{m=-n}^{n} E_{nm}(\omega) h_n^{(2)}(kr) Y_n^m(\theta, \varphi) \tag{5.1}$$

one remembers, that the definition of E_{nm} is still missing. It will be introduced now as a term, that is defined by the boundary values. Like defined above this is in the first case $v(\varphi, \theta)|_{r_0}$ and in the second case $p(\varphi, \theta)|_{r_a}$. Applying a SHT to equation (5.1) yields according to [Pom08]:

$$\psi_{nm}(r) = \int_{\Omega} p(r, \varphi, \theta) Y_n^{m*} d\Omega = E_{nm} h_n(kr). \tag{5.2}$$

---

[1] In the case of particle velocity: $r_a = r_0$

[2] The frequency dependency of E_{nm} subsequently will be omitted for better readability.

43
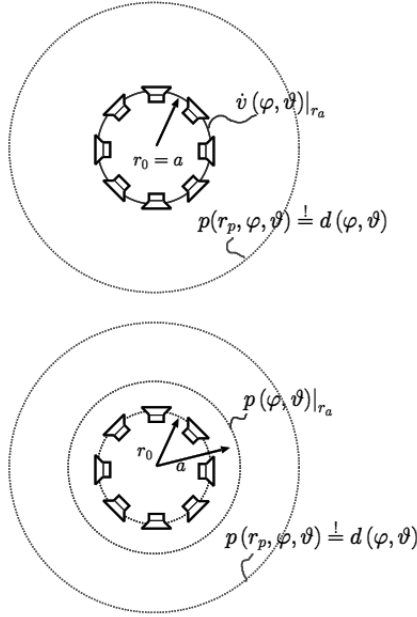
Figure 5.1: the two basic synthesis and analysis arrangements [ZN07]

In [Pom08] and [ZN07] the expressions for the boundary conditions can be found [3]:

a) velocity approach:

$$E_{nm}^{(v)} = i\rho_0 c \cdot \frac{1}{h'_n(kr_0)} \cdot \nu_{nm}\Big|_{r_0}, \tag{5.3}$$

$$\Rightarrow \boxed{\psi_{nm}(r) = i\rho_0 c \cdot \frac{h_n(kr)}{h'_n(kr_0)} \cdot \nu_{nm}\Big|_{r_0}.} \tag{5.4}$$

b) pressure approach:

$$E_{nm}^{(p)} = \frac{1}{h_n(kr_a)} \cdot \psi_{nm}\Big|_{r_a}, \tag{5.5}$$

$$\Rightarrow \boxed{\psi_{nm}(r) = \frac{h_n(kr)}{h_n(kr_a)} \cdot \psi_{nm}\Big|_{r_a}.} \tag{5.6}$$

---

[3]Note, that equation (5.4) is the same, as the one, that was used for the simulation performed in chapter 4 (equation (4.12)).

44

5.2 Beamformer

With beamformer here the control unit is meant that is necessary for system control. It can be split up into two parts:

a) angular beamformer:

Its input are the expansion coefficients of the desired pattern. This can be for example the coefficients of a beam like derived in equation (4.26):

$$\psi_{nm} = Y_n^{m*}(\varphi_b, \theta_b). \tag{5.7}$$

The output of the angular beamformer are the driver voltages, which produce the desired pattern on the analysis radius r_a. This pattern control will be examined closer in section 5.3.

b) radial beamformer:

The pattern produced by the angular beamformer on r_a is projected to the projection radius r_p with the radial beamformer. It can be seen like a pre-filtering, which equalizes the damping of the spherical harmonics according to the propagation term. This filter is also called radial steering filter (RSF) and will be observed in section 5.4. For equalization the reciprocal terms of equations (5.3) and (5.5) are used:

$$H_n^{(eq,v)}(\omega) = -\frac{1}{\rho_0 c} \cdot i \cdot \frac{h_n'(kr_0)}{h_n(kr_p)}, \tag{5.8}$$

$$H_n^{(eq,p)}(\omega) = \frac{h_n(kr_a)}{h_n(kr_p)}. \tag{5.9}$$

Figure 5.2 shows the structure of the entire beamformer. The input signal $x[n]$ can be an arbitrary audio signal, like music, noise or any kind of measuring signal, which is than directed in beam direction.
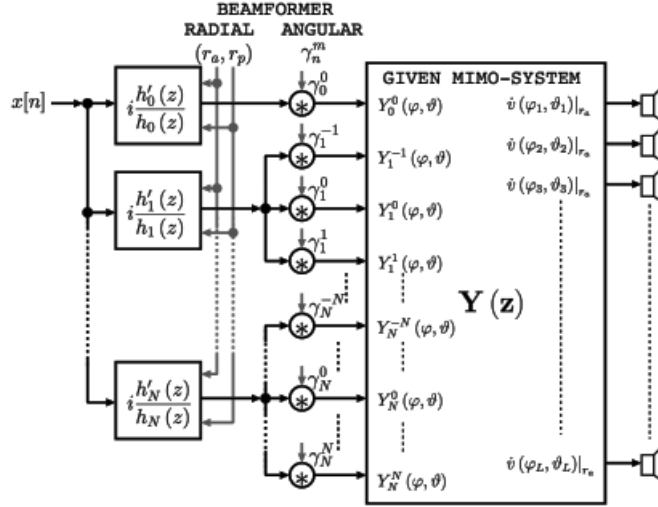
Figure 5.2: structure of the beamformer according to [ZN07]

5.3 Pattern Control

To gain control over the loudspeaker system and be able to create a desired pattern it is necessary to know the active and passive transfer properties of the system (system identification). These can be determined in two ways:

a) by measuring the velocity distribution at r_0 using a Laser Doppler Vibrometer (LDV)

b) by measuring the sound pressure distribution at r_a using a microphone array

Here only the first approach will be described step by step. For the measurement with microphones the interested reader is referred to [Pom08] or [ZPS08].

1. The MIMO-system.   The transfer properties of the array can be described as a MIMO-system[4], which is depicted in figure 5.3. There $t_{ij}(t)$ denotes the time-domain transfer-functions from the i-th to the j-th loudspeaker. Transforming it to the frequency-domain using an FFT yields the frequency response of the active $(i = j)$ and passive $(i \neq j)$ transfer paths. The passive ones describe the mutual crosstalk and occur because of the common enclosure of the loudspeakers.

---

[4]MIMO = Multiple Input Multiple Output
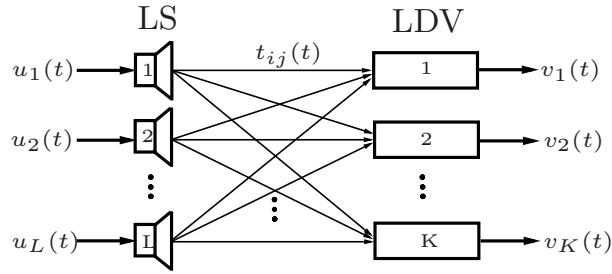
Figure 5.3: The LDV-loudspeaker-MIMO-system, L: No of loudspeakers; K: No of LDV measurement positions

The frequency-domain transfer functions are summarized in a matrix $\mathbf{T}(\omega)$ [5], the so called system matrix. As here $L = K$ it results in a square matrix:

$$\mathbf{T}(\omega) = \begin{bmatrix} t_{11}(\omega) & \dots & t_{1L}(\omega) \\ \vdots & \ddots & \vdots \\ t_{L1}(\omega) & \dots & t_{LL}(\omega) \end{bmatrix}. \tag{5.10}$$

With this definition a vector $\boldsymbol{v}$ containing all the driver velocities can be built out of the corresponding driving voltage vector $\boldsymbol{u}$:

$$\boldsymbol{v} = \mathbf{T} \cdot \boldsymbol{u}, \tag{5.11}$$

with the dimensions:

$$[L \times 1] = [L \times L] \cdot [L \times 1]. \tag{5.12}$$

How the measurements with the LDV can be performed, will be shown in chapter 6. For a first - but highly unrealistic - approach, the system matrix $\mathbf{T}$ can be assumed to be an identity matrix, meaning, that every loudspeaker has a flat frequency response and there is no crosstalk.

2. SH-transform. According to equation (4.13) $\boldsymbol{v}$ can be written as:

$$\boldsymbol{\nu} = \mathbf{A} \cdot \boldsymbol{v}. \tag{5.13}$$

---

[5]The frequency-depencency will be omitted for better readability

A contains the expansion coefficients of the cap model for all L drivers as derived in section 4.1. Putting equation (5.11) into equation (5.13) yields:

$$\boldsymbol{\nu} = \mathbf{A} \cdot \mathbf{T} \cdot \boldsymbol{u}, \tag{5.14}$$

$$[(N+1)^2 \times 1] = [(N+1)^2 \times L] \cdot [L \times L] \cdot [(N+1)^2 \times 1]. \tag{5.15}$$

Note, that the maximal SH-order is $N = 3$ and therefore $(N+1)^2 = L$, which leads to square matrices and therefore exact invertibility [6].

3. Calculation of the driver voltages in SH. Let us assume the loudspeaker signals $u(\Theta)$ as weighted Dirac delta located in the center of each loudspeaker:

$$u(\Theta) = \sum_{l=1}^{L} \delta(\Theta - \Theta_l) \cdot u_l. \tag{5.16}$$

This is quite similar to the approach to gain the velocity distribution for the cap sphere model made in sections 4.1 and 4.2. Assuming that the voltage is transfered directly into velocity one can use equation (4.13) replacing the velocity quantities by voltage quantities and get:

$$\boldsymbol{u_{SH}} := \boldsymbol{\Upsilon} = \mathbf{A} \cdot \boldsymbol{u}, \tag{5.17}$$

$$\Rightarrow \boldsymbol{u} = \mathbf{A}^{-1} \cdot \boldsymbol{\Upsilon}. \tag{5.18}$$

As **A** is square the inverse can be used. $\mathbf{A}^{-1}$ often is called decoder-matrix, because it decodes the SH-domain voltages to real-world voltages, the drivers can be supplied with. Putting equation (5.18) into (5.14) yields:

$$\boldsymbol{\nu} = \mathbf{A} \cdot \mathbf{T} \cdot \mathbf{A}^{-1} \cdot \boldsymbol{\Upsilon}. \tag{5.19}$$

4. Introduction of a control matrix. Equation (5.19) is already a rather good description of the overall system. What is still missing is the desired quantity $\boldsymbol{\gamma}$ given in spherical harmonics coefficients. As proposed in section 5.2 it can be the expansion coefficients of a beam according to equation (5.7) or any arbitrary set of coefficients. A

---

[6]Of course under the precondition that the inverse exists.

control matrix $\mathbf{B}$ is needed, which transforms $\boldsymbol{\gamma}$ into a voltage vector:

$$\boldsymbol{\Upsilon} = \mathbf{B} \cdot \boldsymbol{\gamma}. \tag{5.20}$$

Putting this equation into (5.19) yields the description of the overall sytem:

$$\boxed{\boldsymbol{\nu} = \mathbf{A} \cdot \mathbf{T} \cdot \mathbf{A}^{-1} \cdot \mathbf{B} \cdot \boldsymbol{\gamma}.} \tag{5.21}$$

With the dimensions:

$$[(N{+}1)^2 {\times} 1] = [(N{+}1)^2 {\times} L] \cdot [L {\times} L] \cdot [L {\times} (N{+}1)^2] \cdot [(N{+}1)^2 {\times} (N{+}1)^2] \cdot [(N{+}1)^2 {\times} 1]. \tag{5.22}$$

As we want $\boldsymbol{\nu} \overset{!}{=} \boldsymbol{\gamma}$ in equation (5.21) an identity matrix must be obtained meaning:

$$\mathbf{A} \cdot \mathbf{T} \cdot \mathbf{A}^{-1} \cdot \mathbf{B} \overset{!}{=} \mathbf{I}, \tag{5.23}$$

$$\Rightarrow \boxed{\mathbf{B} = (\mathbf{A} \cdot \mathbf{T} \cdot \mathbf{A}^{-1})^{-1}.} \tag{5.24}$$

5. Calculation of the driver voltages. Now we are ready for the final step. Combining equations (5.18) and (5.20) yields:

$$\boxed{\boldsymbol{u} = \mathbf{A}^{-1} \cdot \mathbf{B} \cdot \boldsymbol{\gamma}.} \tag{5.25}$$

6. Block diagram. Finally a block diagram is given to visualize the transformation of the quantities.
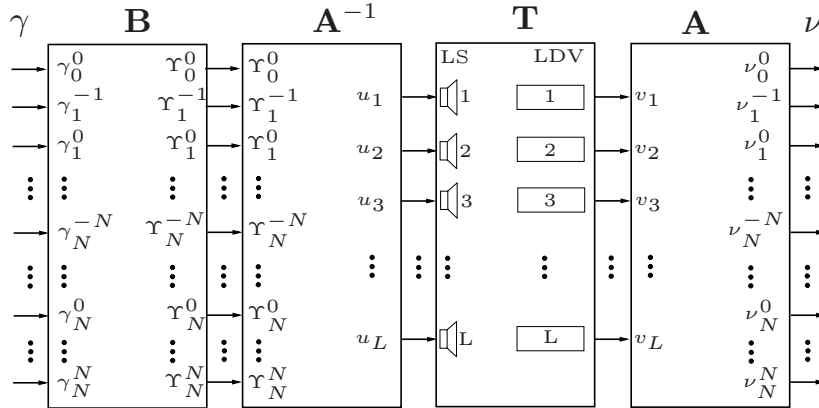
Figure 5.4: block diagram of the angular beamformer

5.4 Radial Steering Filters and Filterbank

According to the propagation term $i\rho_0 c \cdot \frac{h_n(kr_p)}{h'_n(kr_0)}$ in equation (5.4) the SH are attenuated on their way from the array surface r_0 to the projection surface at r_p. The attenuation mainly depends on the design parameter r_0, the frequency and the distance to the array r_p. Figure 5.5 shows the frequency response of the propagation term in the far field.
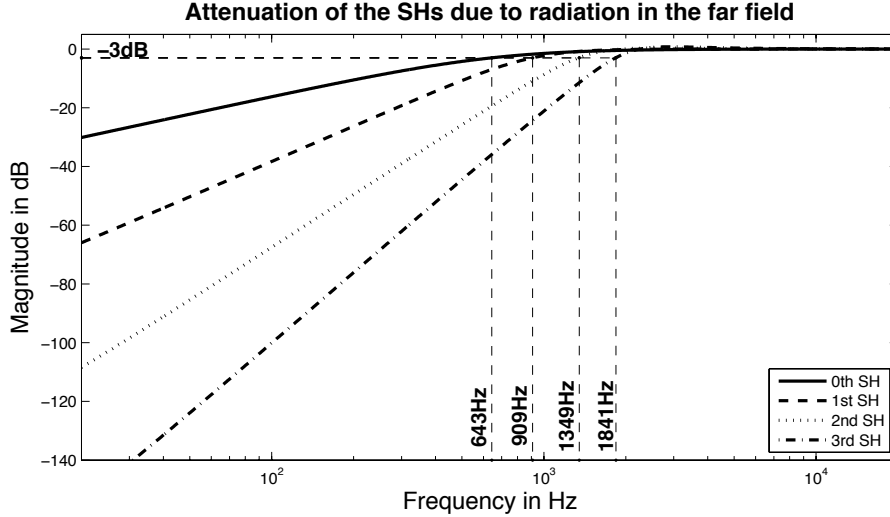
Figure 5.5: Attenuation of the first four SH due to the propagation term

It can be seen, that the SHs are already immensely attenuated at rather high frequencies. As yet proposed in section 5.2 the attenuation could be avoided applying preposed inverse filters, the radial steering filters (RSF). They are based on equations (5.8) and (5.9). A comprehensive filter implementation can be found in [Pom08]. Since these filters in the far field reach unfeasibly high magnitudes up to 140 dB and more, as seen in figure 5.6, the filter gains must be limited.
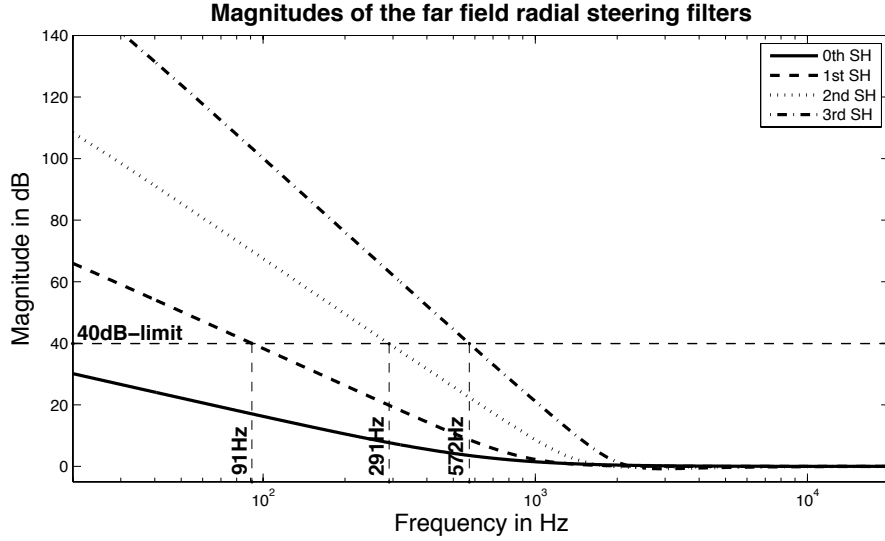
Figure 5.6: far field radial steering filters to compensate the damping of the SH

Limiting the RSF. Let us assume, that the filter curves should be limited to 40dB. This means, that ideally the curves in figure 5.6 should be cut off at the shown frequency positions. Only the 0th SH curve must not be bounded. Doing so, a problem occurs: when coming from high frequencies, for every spherical harmonics order that is omitted, components are missing for the forming of the beam and therefore the magnitude of the beam decreases. The magnitude of a beam can be given by:

$$b_N = \frac{(N+1)^2}{4\pi},$$

(5.26)

where N is the SH-order. The derivation of equation (5.4) is given in appendix B. Every time a spherical harmonic is being faded out due to the RSF, the residual spherical harmonics must be boosted to maintain the magnitude of the beam.

The amplification constants g_N conform to the highest used spherical harmonic (here the 3rd), as using all controllable spherical harmonics defines the maximum magnitude of the beam, which we want to normalize to [7]:

$$g_N = \frac{b_3}{b_N}.$$

(5.27)

---

[7]The denominator in equation (5.4) is omitted, as it is the same value for all spherical harmonics anyway.

The values for b_N and g_N are given in table 5.1.

N	$b_N * 4\pi$	g_N	$g_N[dB]$
0	1	16/1	24
1	4	16/4	12
2	9	16/9	5
3	16	16/16	0

Table 5.1: magnitude of a beam depending on the SH-order N and the according gain values

The Filterbank. As g_N depends on the frequency, it is reasonable to use a filterbank, which amplifies the SH according to the frequency bounds of each filter. The scheme for the filterbank is shown in figure 5.7.
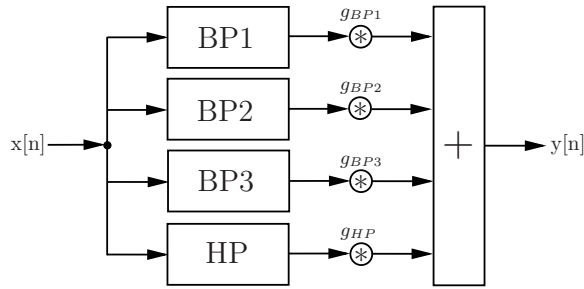
Figure 5.7: schematic configuration of the RSF stabilization filterbank, where the input is a SH of order N and the output is its filtered version

As each SH order should be faded out when reaching the given 40dB bound, it is clear, that the SH order must be filtered with different weights. So the gain values of the lower order SH $n < N$ are set to zero. Table 5.2 shows the complete set of gains for each SH order:

N	g_{BP1}	g_{BP2}	g_{BP3}	g_{HP}
0	16	4	16/9	1
1	0	4	16/9	1
2	0	0	16/9	1
3	0	0	0	1

Table 5.2: list of the gains for each SH order

What is still missing are the frequency bounds for the filters. Since the flterbank amplifies each order, the 40dB frequency bounds of figure 5.6 cannot be used, as the 40dB limit would be exceeded. Therefore the amplification is taken into account before the filterbank. The borders thus are set $g_N[dB]$ below the 40dB-level. This is shown in figure 5.8.
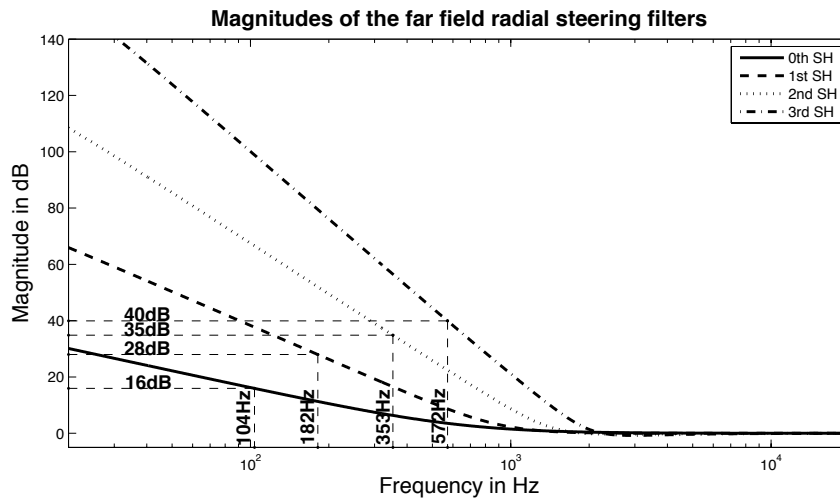
Figure 5.8: cutoff frequencies for the filterbank according to their gain value

Now all relevant information for the design of the filterbank is collected. In figure 5.9 a possible implementation using 3rd order Butterworth-bandpass-filters and a 5th order Butterworth-highpass is depicted.
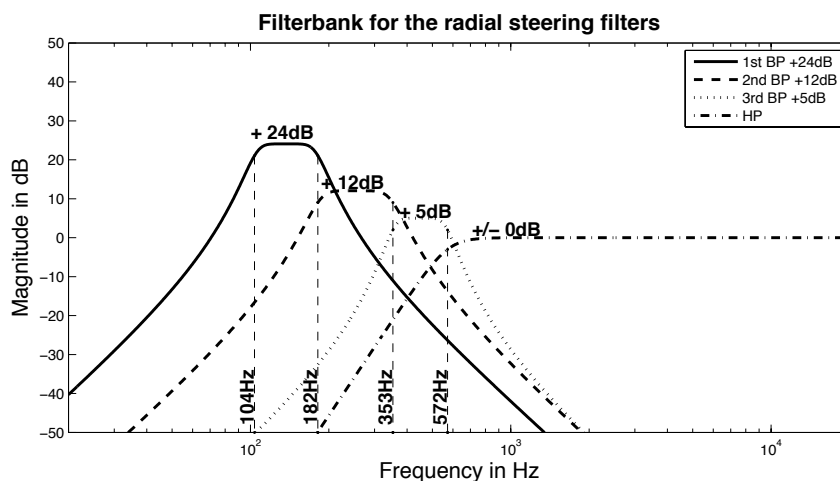
Figure 5.9: filterbank preposed to the radial steering filters

53

Figure 5.10 shows the filter curves as employed to each spherical harmonic.
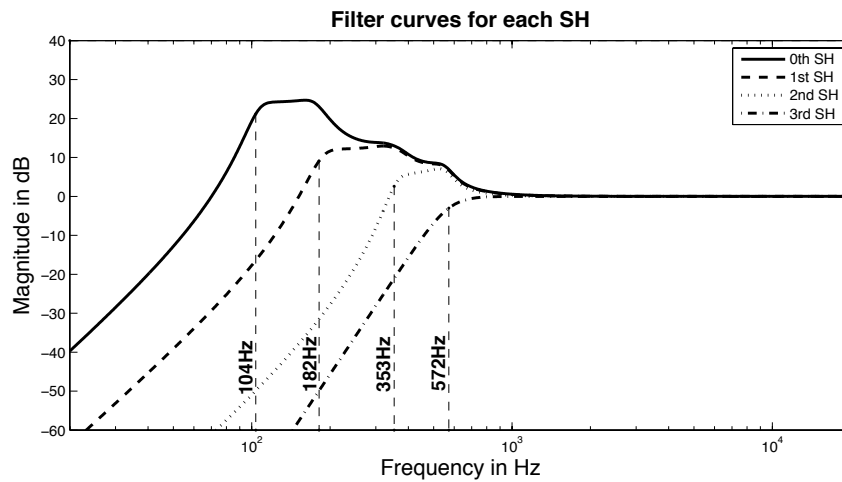
Figure 5.10: filter curves for the first four SHs

The limited RSF. Finally the filterbank is applied to the RSF. Figure 5.11 shows, that all SH are bounded to the given 40dB-limit.
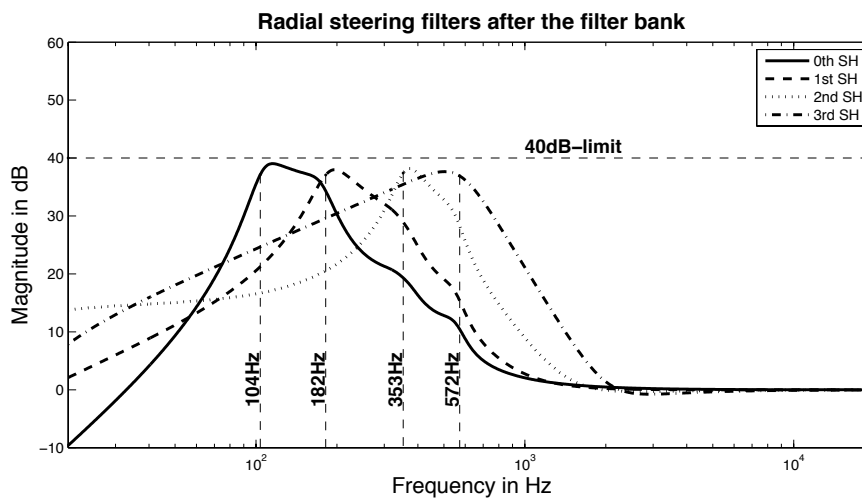
Figure 5.11: limited radial steering filters

The purpose of the derived filters is to obtain a flat frequency response for the beam amplitude. Referring to appendix B equation for the beam amplitude can be written as:

$$b_N = \sum_{n=0}^{N} \frac{2n+1}{4\pi}. \tag{5.28}$$

54

Let us assume that h_n denotes the propagation term and $\tilde{h}_n^{-1} = \frac{h_{fb,n}}{h_n}$ the term for the filtered radial steering filters, with $h_{fb,n}$ being the filter curves for the SHs, as shown in figure 5.10. Bringing these terms into equation (5.28) yields:

$$b_N = \sum_{n=0}^{N} h_n \tilde{h}_n^{-1} \frac{2n+1}{4\pi}. \tag{5.29}$$

Taking into account, that the unfiltered radial steering filters, which are part of $\tilde{h}_n^{-1}$, completely equalize the propagation term, only the filter curves for the SHs $h_{fb,n}$, remain in equation (5.29) and we obtain:

$$b_N = \sum_{n=0}^{N} h_{fb,n} \frac{2n+1}{4\pi}. \tag{5.30}$$

Figure 5.12 shows the frequency response of the beam amplitude. It can be seen, that it is completely flat above about 700 Hz. From 200 Hz to 700 Hz a slight ripple can be observed and below 200 Hz the beam amplitude fades out. This means, that the filterbank is not able to linearize the frequency response of the beam amplitude completely, but above 200 Hz it can be regarded as quasi-constant. Nevertheless, the filterbank provides a reliable limitation of the filters.
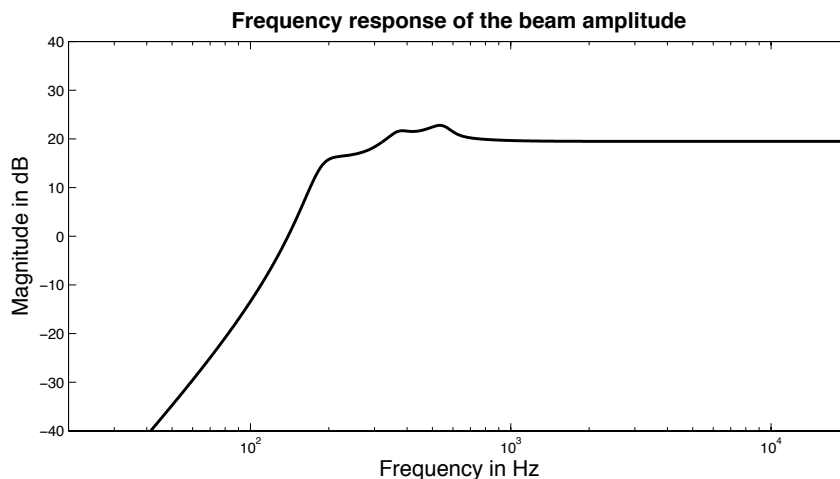
Figure 5.12: frequency response of the beam amplitude employing the filterbank

Chapter 6

System Identification using LDV-Measurements

This chapter deals with the identification of the MIMO-system the spherical loudspeaker array is representing as shown in figure 5.3, in particular, the determination of the active and passive transfer paths of the loudspeakers with a Laser Doppler Vibrometer (LDV). This is a measuring tool that can determine the surface velocity of a vibrating surface - here the loudspeaker membranes.

6.1 Exponential Sweep Measurement Method

There are several methods of system identification like direct impulse response measurements, one- and two-path-FFT measurements, Time-Delay-Spectrometry (TDS), Maximum Length Sequence (MLS) and swept sine methods. Basic descriptions of these methods are found in [Maj07]. Here the logarithmic swept sine technique is used. It has the great advantage, that the detection of harmonic distortions is easy. Furthermore the generation of the signal is quite simple. Farina gives a comprehensive description of this method in [Far00].

Sweep Generation. The sweep signal was generated in MATLAB. The instantaneous frequency is given by:

$$\omega(t) = \left(\frac{\omega_2}{\omega_1}\right)^{\frac{t}{T}} \cdot \omega_1, \tag{6.1}$$

where ω_1 and ω_2 are the start and stop frequencies of the sweep and T the sweep time.

Taking the logarithm and rearranging the terms in this formula yields the design equation for the group delay of the sweep [JR07]:

$$n(\omega) = \frac{ln(\frac{\omega}{\omega_1})}{ln(\frac{\omega_2}{\omega_1})} \cdot (N - 1), \tag{6.2}$$

with N being the sweep length in samples. This group delay is used for a frequency-domain based sweep design. Furthermore this sweep is filtered with a band-pass to avoid transient oscillations. Figure 6.1 shows the used sweep with an active length of $N = 44100$ and the cut-off frequencies $f_1 = 80Hz$ and $f_2 = 18kHz$, in the time and in the frequency domain.
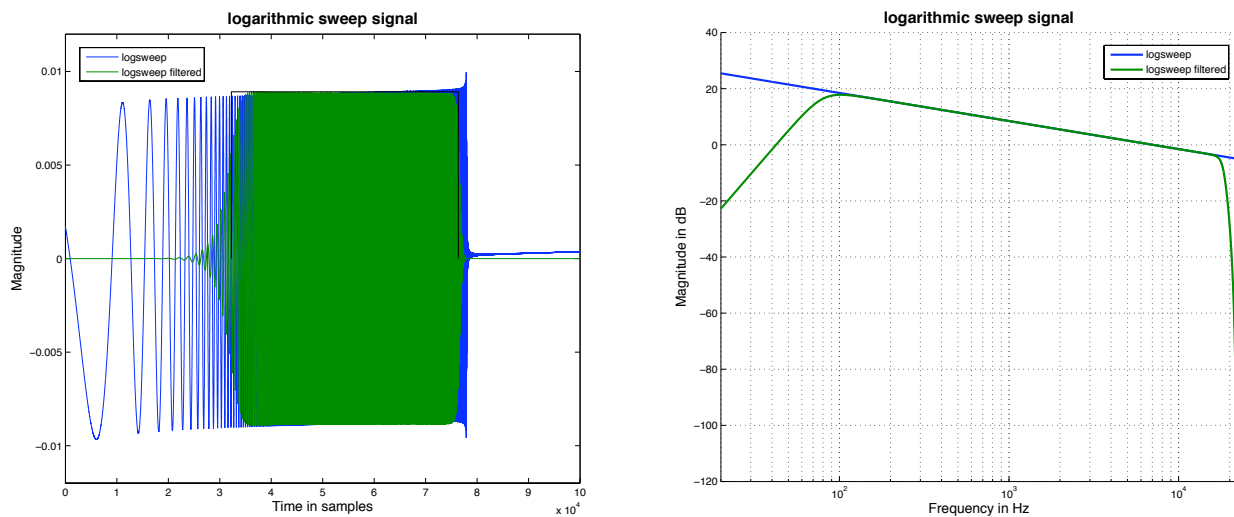
Figure 6.1: time and frequency domain logarithmic sweep signals
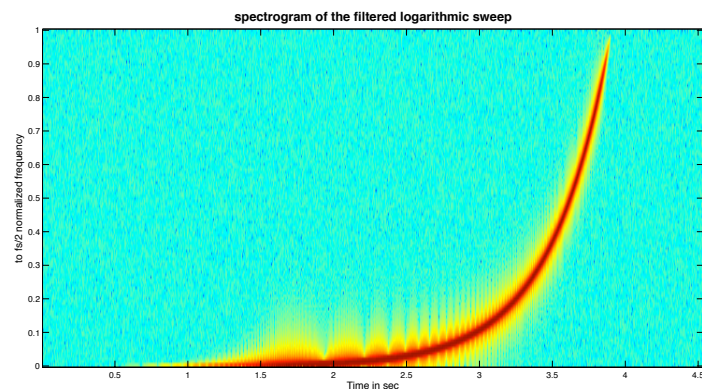
Figure 6.2: spectrogram of the logarithmic sweep signal

6.2 Measurement Setup

Figure 6.3 shows the setup for the measurements. A PD-patch [1] controls the playback of the sweep signal that is sent to a digital-analog-converter and then amplified. The loudspeaker movement is detected with the LDV. The focused laser of the LDV points to the center of one loudspeaker membrane and the remaining loudspeakers play back the sweep signal one after another. This is repeated for all loudspeakers. The measured LDV-output-signal is transformed back to the digital domain with an analog-digital-converter and finally recorded again in PD.
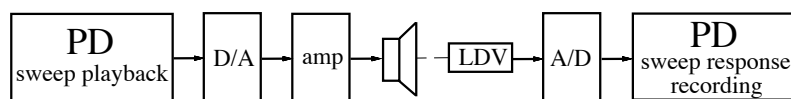
Figure 6.3: block diagram of the measurement setup

Figure 6.4: measurement setup in the IEM-library consisting of the spherical loudspeaker array, the LDV and the rack in the background containing the AD- and DA-converters, the amplifiers and the computer for PD

---

[1] PD is the abbreviation for Pure-Data, a real-time audio programming software by Miller S. Puckette.

According to the LDV-manual [LDV] the best measurement distances are:

$$a = 96mm + n \cdot 138mm; n = 0, 1, 2....$$
(6.3)

For the measurements a distances of 510 mm was chosen. An advantage of the LDV-approach is, that the influence of the room on the measurements is more or less negligible, although a suitable environment should be given, as the LDV is very sensitive to vibrations. As the LDV only measures the membrane velocity, it does not regard sound radiation. Therefore, the interpretation is not as straightforward, as for example sound pressure level frequency responses [2]. A disadvantage of the swept sine method is, that transient disturbances can cause problems.

6.3   Measurement Evaluation

Calculation of the transfer function.   The sweep signal x and the measured sweep responses y_{ij} from the j-th to the i-th loudspeaker are first brought to the frequency domain by FFT:

$$X(\omega) = FFT(x[n]),$$
(6.4)

$$Y_{ij}(\omega) = FFT(y_{ij}[n]).$$
(6.5)

For the derivation of the transfer function the following nomenclature and definitions are used [3]:

H_{ij}: transfer function

X: unfiltered sweep signal

Y_{ij}: measured system response

B: band-pass filter

$\tilde{X}$: band-pass filtered sweep signal (used as playback signal in the measurements)

$\tilde{H}_{ij}$: band-limited transfer function

---

[2]Like the one in appendix A

[3]Note, that all quantities depend on the frequency, which is again omitted for better readability.

$$Y_{ij} = H_{ij} \cdot \tilde{X}, \tag{6.6}$$

$$\tilde{X} = B \cdot X. \tag{6.7}$$

The transfer function shall be band-limited to limit the duration of the sweep especially at low frequencies. Furthermore, without the band-pass an overshoot caused by Gibbs phenomenon could emerge at the lower and higher cut-off frequency. As we want a pink spectrum, this must be avoided.

$$\tilde{H}_{ij} \overset{!}{=} H_{ij} \cdot B = \frac{H_{ij} \cdot (B \cdot X)}{X} \tag{6.8}$$

Note, that the denominator in equation (6.8) is the unfiltered version of the sweep. Hence, an amplification of the noise that occurs when dividing by very small numbers outside the measurement frequency range is avoided.

Cutting the impulse responses. The impulse response (IR) h_{ij} is calculated by an Inverse Fast Fourier Transform (IFFT) of $\tilde{H}_{ij}$ using the FFT-length of equation (6.5). Figure 6.5 depicts the IR of the active transfer path of the first loudspeaker. It shows, that noise is present in the measurement and that there are harmonic distortions (rear part of the IR). As we are not interested in these disturbances, the IRs must be windowed.
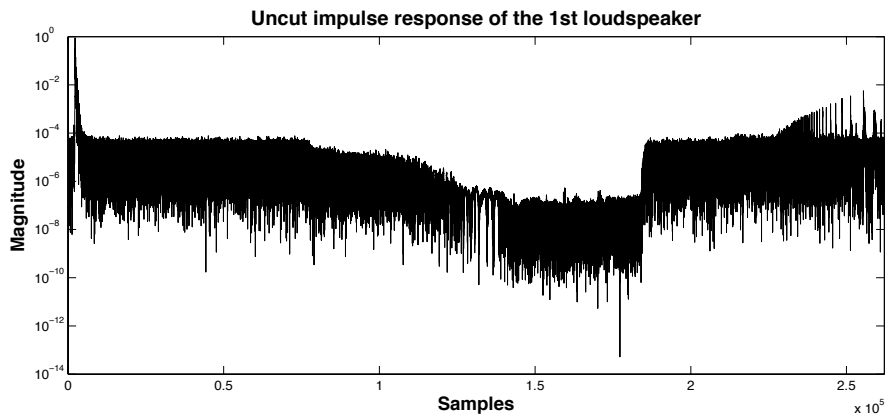
Figure 6.5: uncut impulse response for the northpole-speaker with logarithmic y-axis

To avoid transient cutting, the first half of a 200-point Hanning window is used for fade-in and the second half of a 1500-point Hanning window for fade-out. The remaining parts outside the fade-in and fade-out area are thrown away. This editing results in an IR

of 4501 samples. Figure 6.6 shows the result again for the first loudspeaker. The windowing was applied to all 256 IRs.
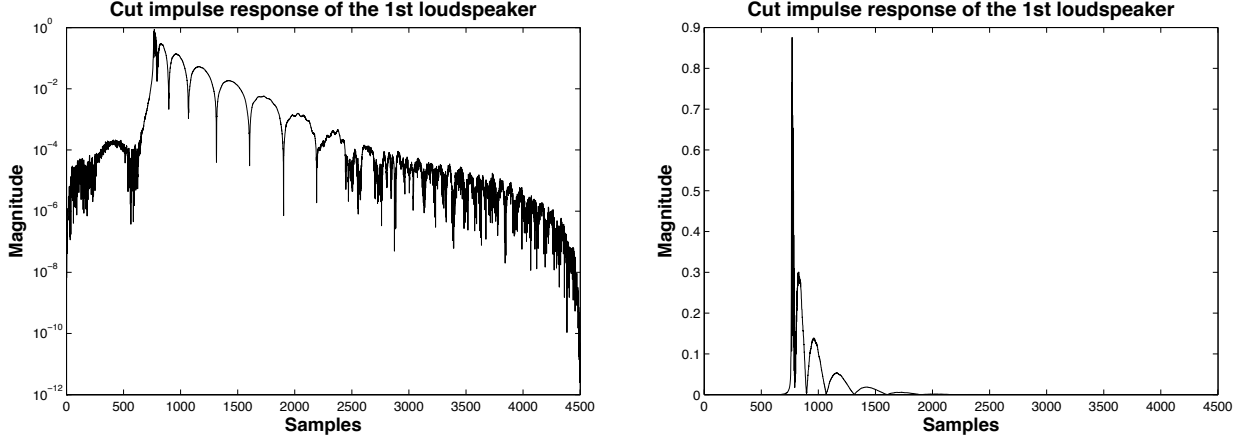
Figure 6.6: cut impulse response of the northpole speaker with logarithmic (left) and linear (right) y-axis

The active paths. Figure 6.7 depicts the magnitude of the frequency responses of the directly driven loudspeakers. They show some peaks at around 1500 Hz, which could be due to resonances in the cabinet. The leap at about 12 kHz may result from higher modes of the membrane surface.

Figure 6.8 shows the differences in the magnitudes of the loudspeakers' frequency responses as deviation from the first speaker. Accordingly the loudspeakers match rather well in the frequency range of interest of about 100 Hz to 3000 Hz.

The angular distance classes. Section 3.3 showed the geometrical properties of the array. It pointed out, that there are several kinds of symmetry and repetition. This information is useful here as it allows us to classify the measured data into angular distance classes. An angular distance class contains all pairs of loudspeakers, that have the same angular distance. These angles can be calculated with the inner product of the direction vectors of two loudspeakers:

$$\cos(\alpha) = \frac{\vec{a} \cdot \vec{b}}{|\vec{a}| \cdot |\vec{b}|}. \tag{6.9}$$
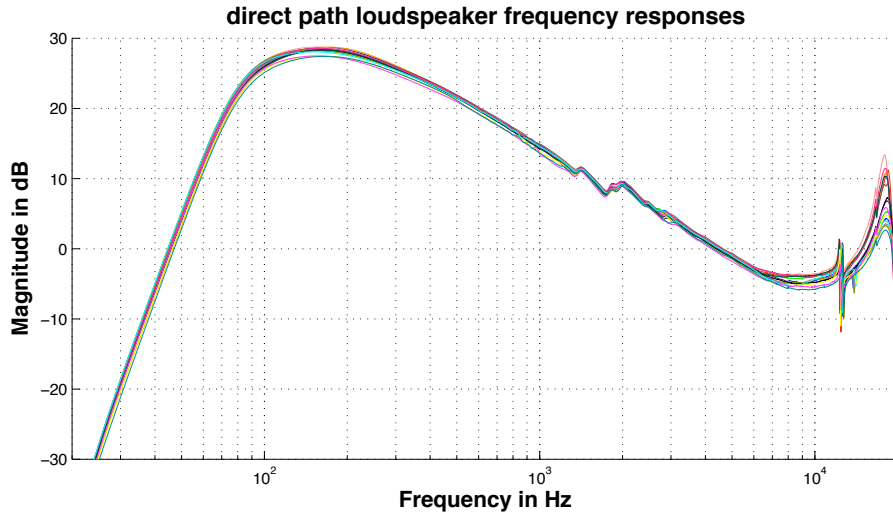
Figure 6.7: velocity frequency response of the 16 loudspeakers
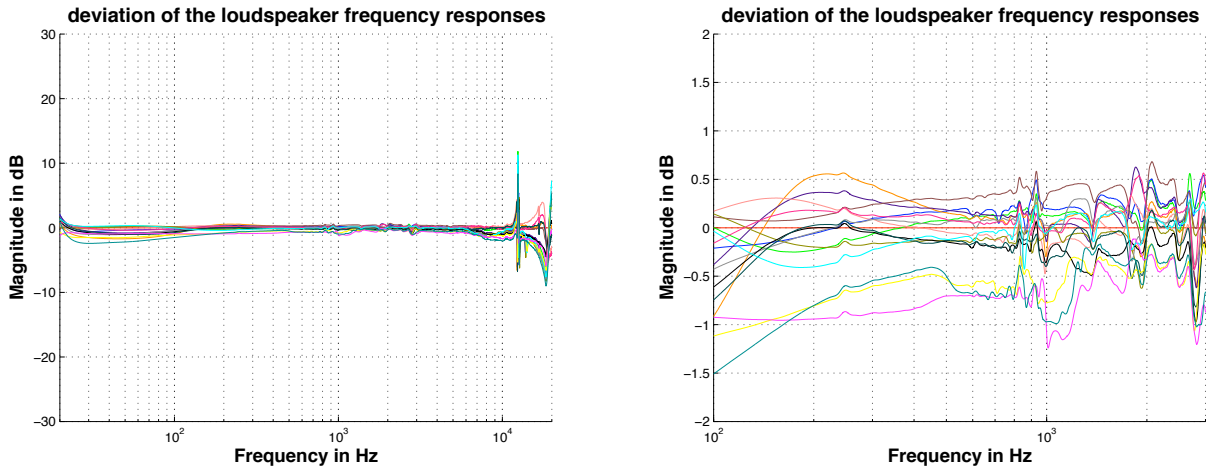
Figure 6.8: spreading in the magnitude of the loudspeaker frequency responses

As normalized vectors are used for calculation and hence $|\vec{a}| = |\vec{b}| = 1$, equation (6.9) simplifies to:

$$\cos(\alpha) = \vec{a} \cdot \vec{b} \Rightarrow \alpha = \arccos(\vec{a} \cdot \vec{b}). \tag{6.10}$$

Performing this calculation for all 16 points yields 256 angles. Sorting the results reveals, that there are 10 angular classes, whereas one is the class of the angle of each loudspeaker with itself. As this class yields an angle of 0° it is denominated as class_0. The other 9 classes and their angles are:

class	angle	polygon to polygon	number
1	50°	5 to 5	12
2	51°	5 to 5	24
3	58°	5 to 6	48
4	95°	5 to 5	48
5	100°	5 to 6	24
6	109°	6 to 6	12
7	117°	5 to 5	24
8	145°	5 to 5	24
9	150°	5 to 6	24

Table 6.1: The angular distance classes with their angle, the sort of polygons, containing the loudspeakers (5: pentagon, 6: hexagon), and the number how many of this constellations exist

The following plots (figure 6.9) depict the magnitudes of the transfer function for every angular class. Class_0 contains the active paths for all 16 loudspeakers and the residual classes the passive paths. All plots are normalized to the maximum of the active paths.

Generally the plots of the passive paths can be divided into four regions with the approximate limits:

1. lower end to 800 Hz: passive loudspeaker movement according to the movement of the air in the cabinet caused by the active loudspeaker portioned to the remaining 15 loudspeakers yielding $20 \log(\frac{1}{15}) = -23.5 dB$

2. 800 Hz to 1.2 kHz: transition section with rather complicated transfer patterns; no proper explanation for this behavior could be found until now

3. 1.2 kHz to 3 kHz: range of resonances in the cabinet

4. 3 kHz to upper end: virtually no crosstalk, only noise is present

Note, that in the 4th region there are some configurations that seem to produce crosstalk. I have not found a good explanation for that. Maybe there was less noise in the measurement.
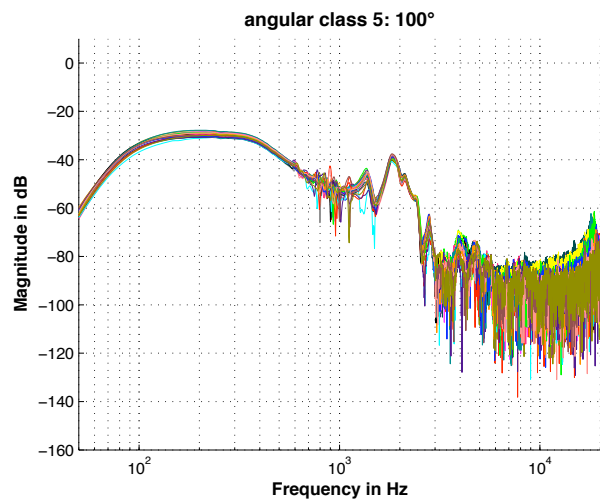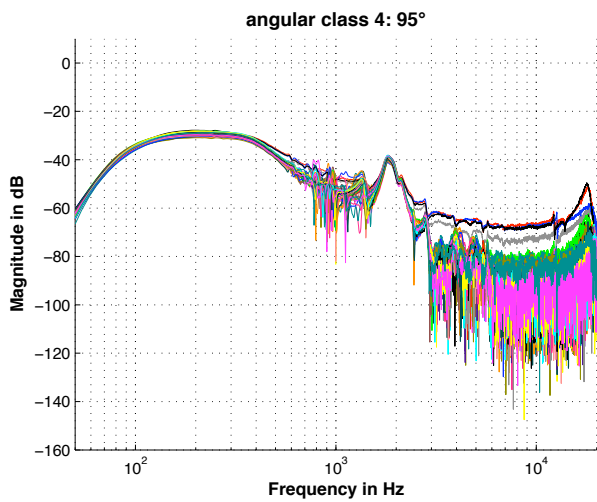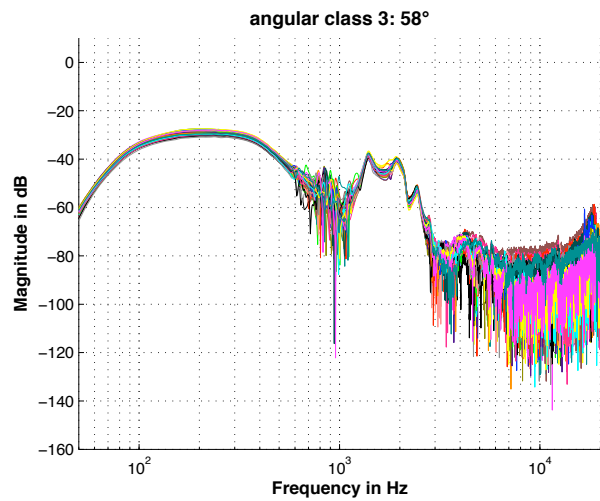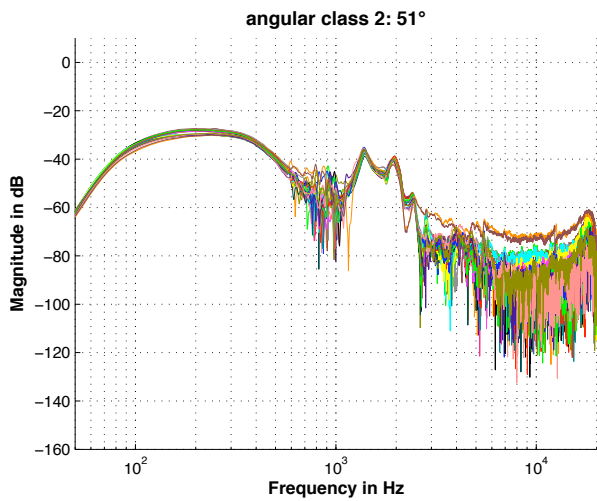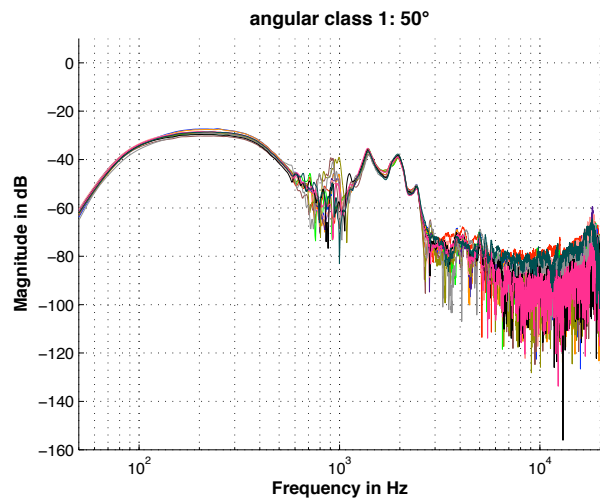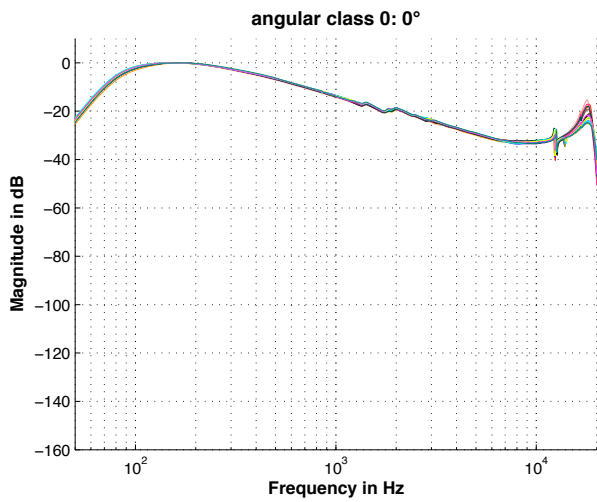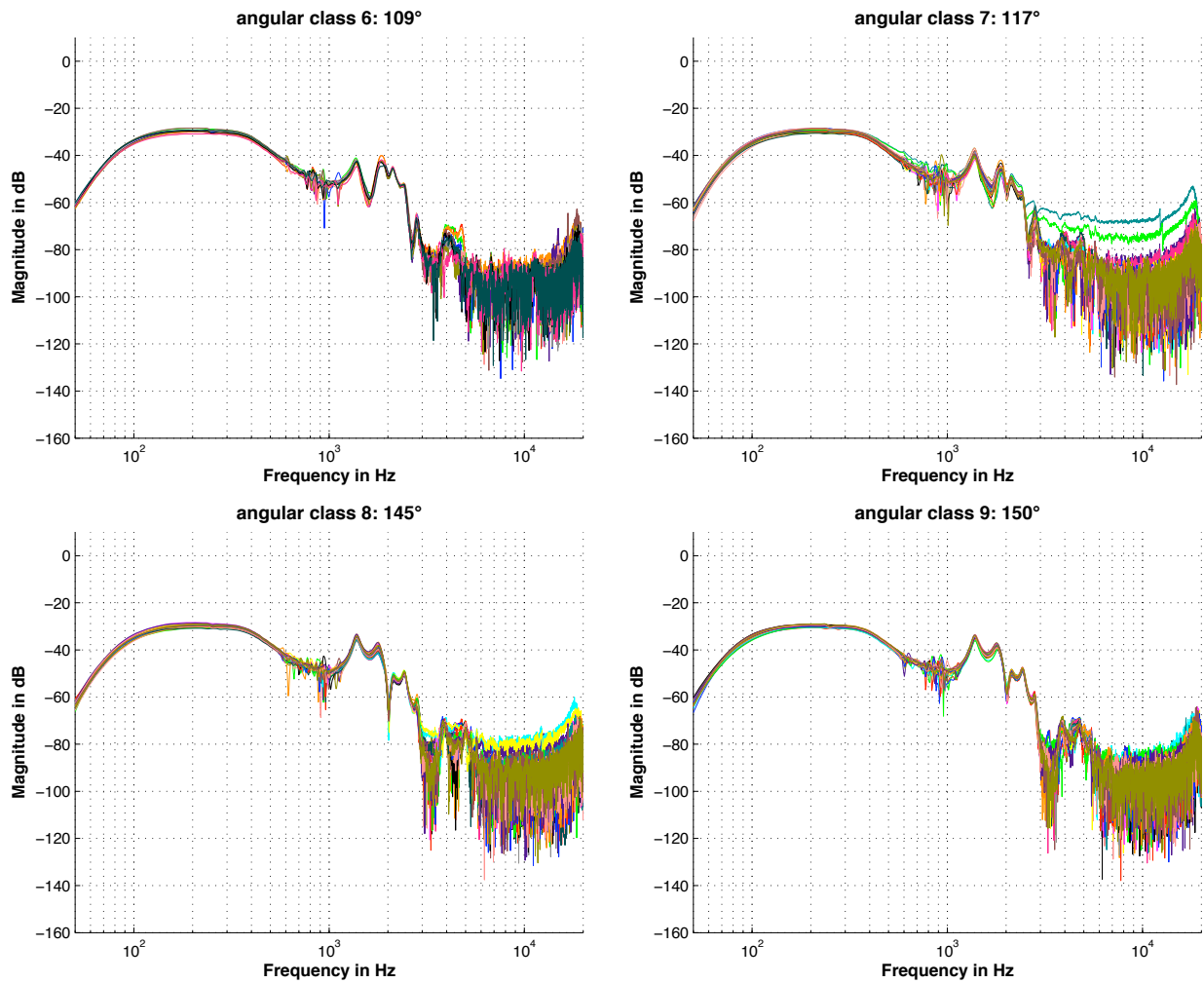
Figure 6.9: magnitude of the frequency responses of all 10 angular classes

Figure 6.10 shows the average attenuation of the passive transfer paths with respect to the average active transfer path. The natural attenuation of the crosstalk is rather good. There are two minima: the first one with 22.3 dB at 1381 Hz and a second one with 21.7 dB at 1822 Hz. These minima might be the main resonances in the cabinet.
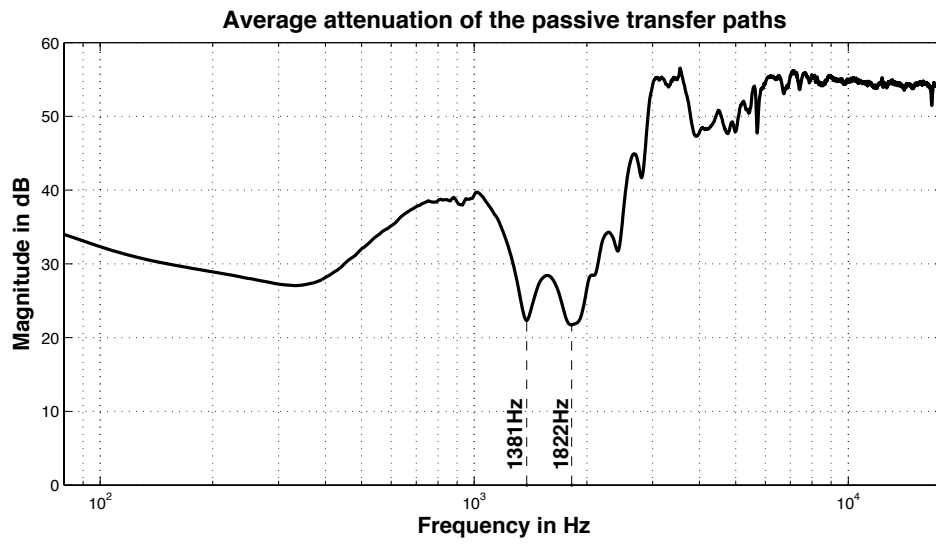
Figure 6.10: average attenuation of the passive transfer paths

Chapter 7

Conclusion and Outlook

In this thesis a spherical loudspeaker array with a new kind of loudspeaker arrangement was developed, built and simulated. It was shown, how an algorithm for system control can be implemented and how the system can be identified using LDV-measurements.

The array uses 16 loudspeakers and therefore the same number of loudspeakers then controllable spherical harmonics in a system of order 3. The arrangement of the drivers was laid out according to a set of extremal points for hyperinterpolation, which solves the task of sound field synthesis in a unique way. The array has rather small dimensions and is therefore suitable for the mid-frequency range. Simulations showed, that the chosen array is able to reproduce the spherical harmonics - and therefore arbitrary band-limited patterns - rather well up to a frequency of about 2500 Hz. Also a beam in a specified direction was simulated. The developed control system consists of angular and radial filters. The radial part contains the radial steering filters, which equalize the attenuation of the spherical harmonics due to radiation. However, these filters come with no stability issues. Therefore a filterbank was developed that limits these filters to a magnitude of 40dB. For an appropriate angular control a profound description of the system's transfer properties is necessary. The determination of these properties was performed with LDV-measurements. It turned out that the magnitudes of the frequency responses of the directly driven loudspeakers in the regarded frequency range of about 100 Hz to 3 kHz match quite well and that the attenuation of the passive paths is rather good.

Outlook:

The array's capability of reproducing a desired pattern was only shown in simulations. It would be interesting to compare the simulation results with a pattern, that was really reproduced by the array. For example, this could be done using Hohl's spherical microphone array. After recording the created pressure pattern with the microphone array, a spherical harmonics analysis could be performed. This way, the difference between the simulated and the measured sound pressure values could be determined.

There are still a lot of other interesting challenges in the field of spherical sound reproduction. To evaluate the quality of the reproduced sound field in comparison with the original sound, psycho-acoustic tests should be performed. Also the influence of several factors - e.g. spatial aliasing - on the human perception are of great interest.

Recently efforts were started, how an alternative mathematical description of the sound field could be made without the usage of spherical harmonics.

Appendix A

The Peerless 830983 Drivers

Here some Thiele-Small-parameters and electrical data of the used drivers due to the data sheet [Thy] are given:

Name	Value
Moving Mass m	1,5 g
Mechanical Q-factor Q_{ms}	3,06
Electrical Q-factor Q_{es}	0,7
Total Q-factor Q_{ts}	0,57
Suspension Compliance C_{ms}	0,76 mm/N
Voice Coil Inductance L	0,2 mH
DC Resistance R	3,8 Ω

Table A.1: some data of the Peerless drivers
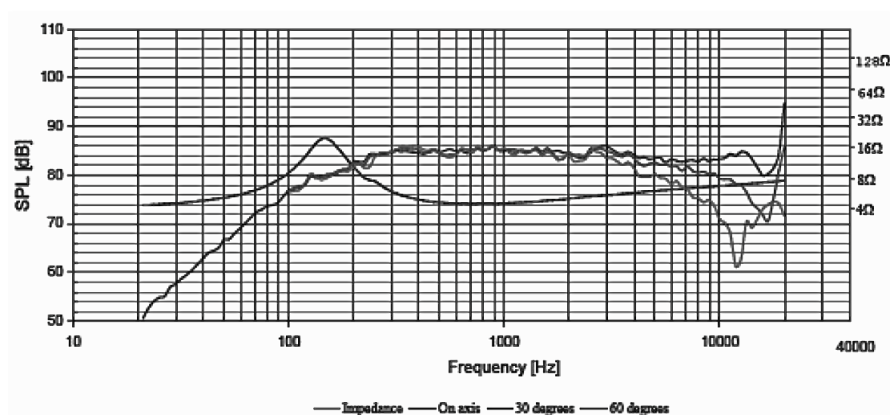
Figure A.1: Pressure frequency response of the used Peerless drivers [Thy]

Appendix B

Derivation of the Beam Magnitude b_N

First we will take a look equation (4.26). It points out, that the expansion coefficients of a beam are the values of the evaluated spherical harmonics at the beam position [1]

$$\chi_{n,B}^m = Y_n^m(\varphi_B, \theta_B). \tag{B.1}$$

Let us assume a beam that originates from the north pole. Therefore the zenith angle $\theta_B = 0$. As the form of the beam may not change in any other direction, the result will be valid for any beam. As we regard a beam from the north pole, all spherical harmonics that have no part pointing to the north are zero and therefore $m = 0$:

$$\chi_{n,BNP}^0 = Y_n^0(\varphi, 0). \tag{B.2}$$

The spherical harmonics can be calculated with equation (2.10):

$$Y_n^m(\varphi, \theta) = \sqrt{\frac{2n+1}{4\pi} \frac{(n-m)!}{(n+m)!}} P_n^m(\cos\theta) e^{jm\varphi}. \tag{B.3}$$

With $m = 0$ and $\theta = 0$ we obtain:

$$Y_n^0(\varphi, 0) = \sqrt{\frac{2n+1}{4\pi}} \cdot P_n^0(1) \cdot 1. \tag{B.4}$$

---

[1]Note, that here the conjugate is omitted due to the usage of real-valued spherical harmonics.

As $P_n^0(1) = 1$, $\forall n$ (cf. [Wil99]) equation (B.4) simplifies to:

$$Y_n^0(\varphi, 0) = \sqrt{\frac{2n+1}{4\pi}}.$$ (B.5)

Regarding equation (B.2) yields:

$$\boxed{\chi_{n,BNP}^0 = Y_n^0(\varphi, 0) = \sqrt{\frac{2n+1}{4\pi}}.}$$ (B.6)

Finally an inverse spherical harmonics transform according to equation (2.17) must be performed:

$$\begin{aligned}
b_N &= ISHT\{\chi_{n,BNP}^0\} = \\
&= \sum_{n=0}^{N} \sum_{m=-n}^{n} \chi_{n,BNP}^0 \cdot Y_n^0(\varphi, 0) = \\
&= \sum_{n=0}^{N} \sqrt{\frac{2n+1}{4\pi}} \cdot \sqrt{\frac{2n+1}{4\pi}} = \\
&= \sum_{n=0}^{N} \frac{2n+1}{4\pi} = \frac{(N+1)^2}{4\pi} \quad q.e.d.
\end{aligned}$$ (B.7)

Appendix C

Spherical Harmonics Simulation

As shown in section 4 the radiation of the spherical harmonics can be simulated using the spherical cap model. The calculation of $\boldsymbol{Q}^{-1}$ can be performed including higher order harmonics or in the truncated subspace only including the controllable spherical harmonics. All calculations where made for nine frequencies: 250Hz, 750Hz, 1500Hz, 2000Hz, 2500Hz, 3000Hz, 5000Hz, 7500Hz and 10000Hz. For the calculation of the cap sphere model a maximum oder of $nmax = 30$ was used.

C.1   Higher Order Harmonics Calculation

First the nine plots for the calculation including the higher order harmonics are depicted:

The first 16 SH at r_a=1m, f=250Hz, nmax=30
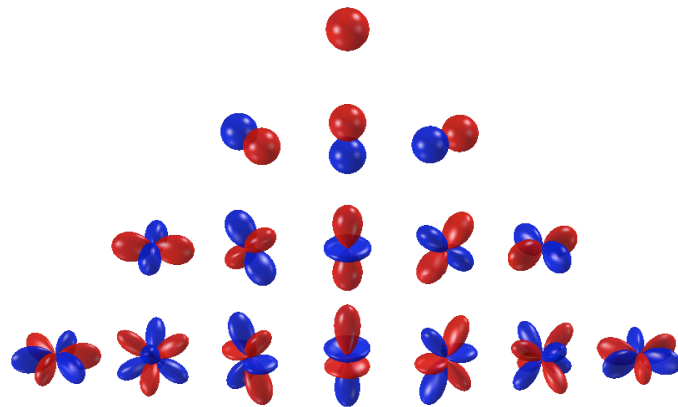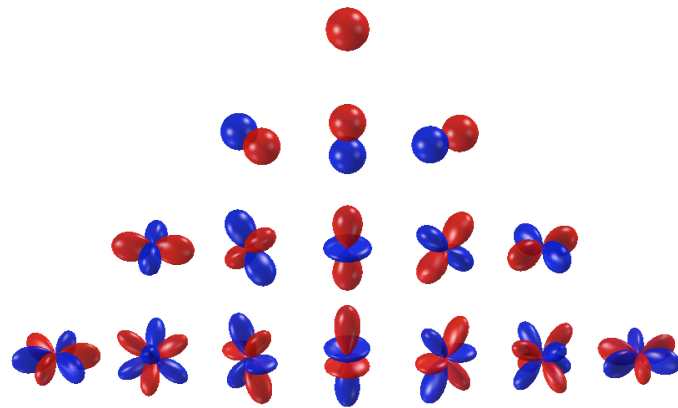
The first 16 SH at r_a=1m, f=750Hz, nmax=30

The first 16 SH at r_a=1m, f=1500Hz, nmax=30
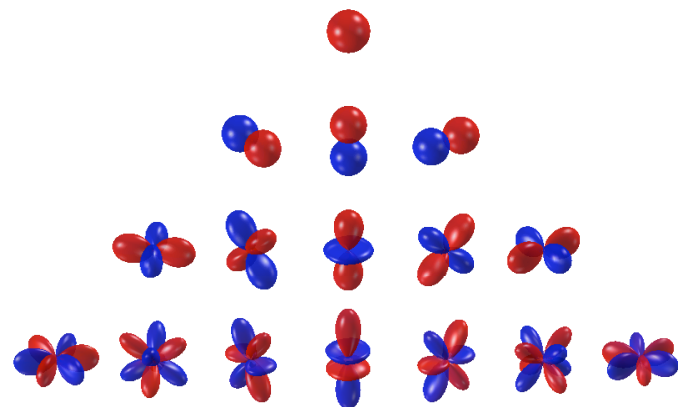
The first 16 SH at r $_a$=1m, f=2000Hz, nmax=30
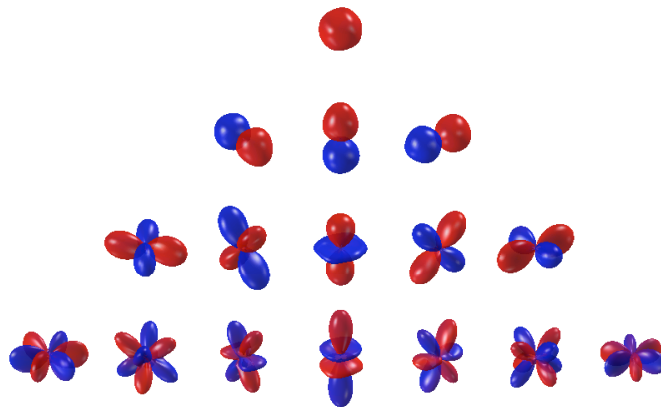
The first 16 SH at r $_a$=1m, f=2500Hz, nmax=30
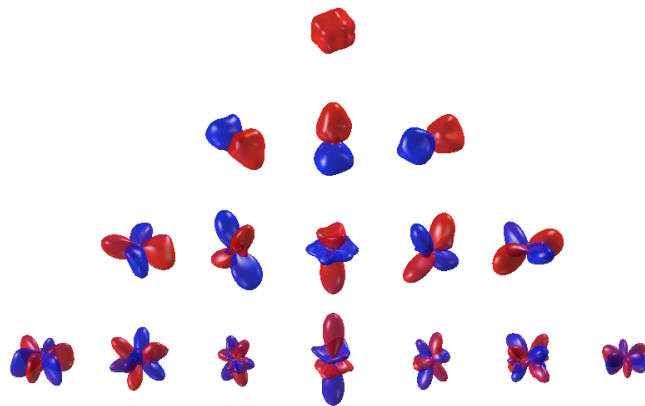
The first 16 SH at r $_a$=1m, f=3000Hz, nmax=30
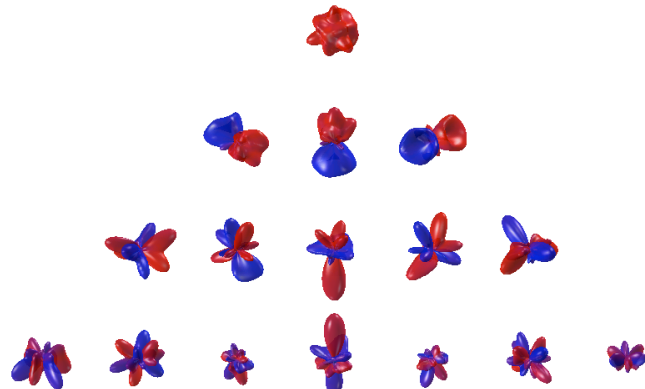
The first 16 SH at r $_a$=1m, f=5000Hz, nmax=30
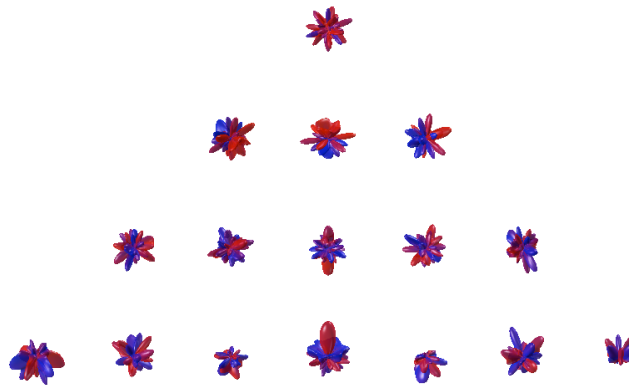
The first 16 SH at r $_a$=1m, f=7500Hz, nmax=30
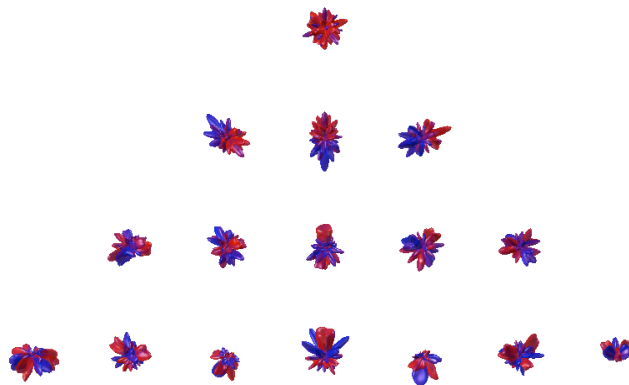
The first 16 SH at r $_a$=1m, f=10000Hz, nmax=30
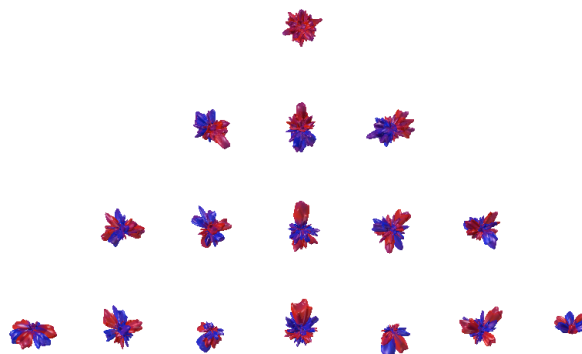
Figure C.1: Higher order calculation

C.2 Truncated Subspace Calculation

And now the same for the truncated subspace. Note, that the spherical harmonics in the first plots seem to be smaller then the ones for the higher order calculation in figure C.1, but in fact they are not. Only the axis was chosen differently to fit for the big values obtained for higher frequencies.

The first 16 SH at r $_a$=1m, f=250Hz, nmax=30
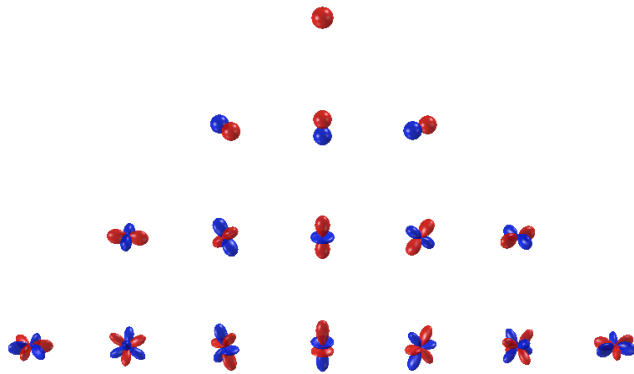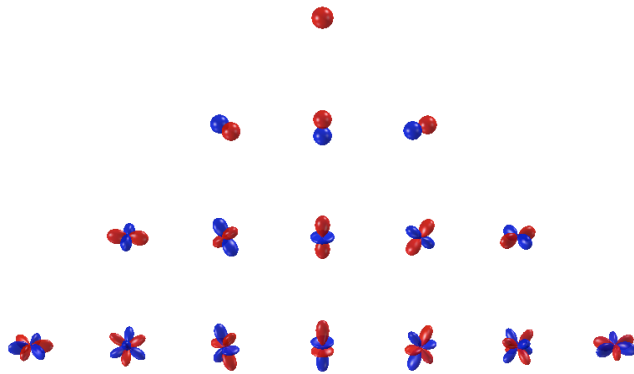
The first 16 SH at r $_a$=1m, f=750Hz, nmax=30

The first 16 SH at r $_a$=1m, f=1500Hz, nmax=30
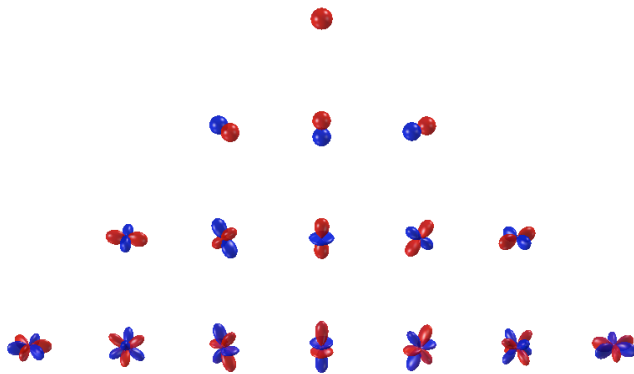
The first 16 SH at r $_a$=1m, f=2000Hz, nmax=30
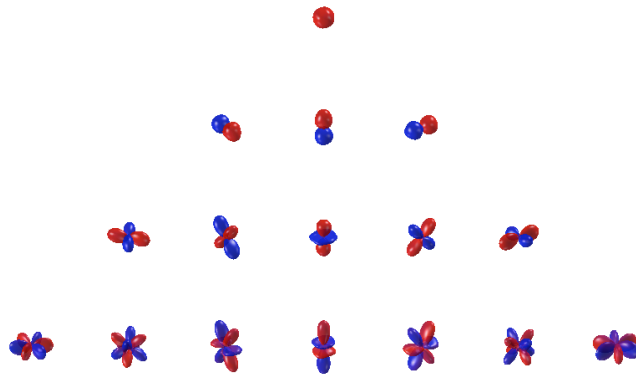
The first 16 SH at r $_a$=1m, f=2500Hz, nmax=30
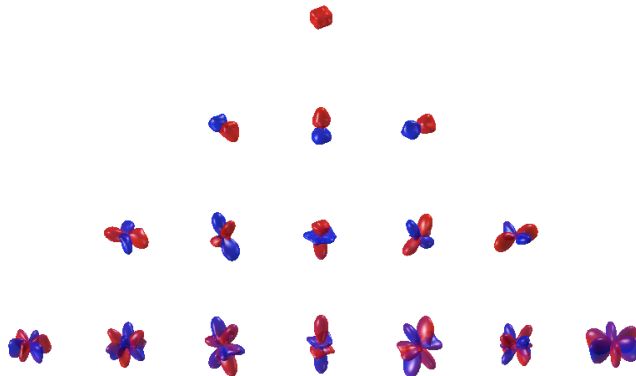
The first 16 SH at r $_a$=1m, f=3000Hz, nmax=30
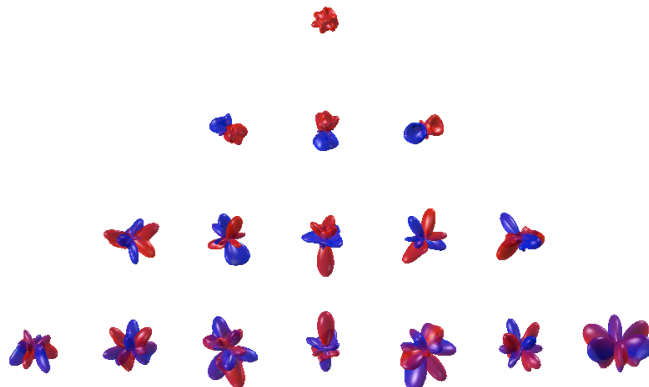
The first 16 SH at r $_a$=1m, f=5000Hz, nmax=30
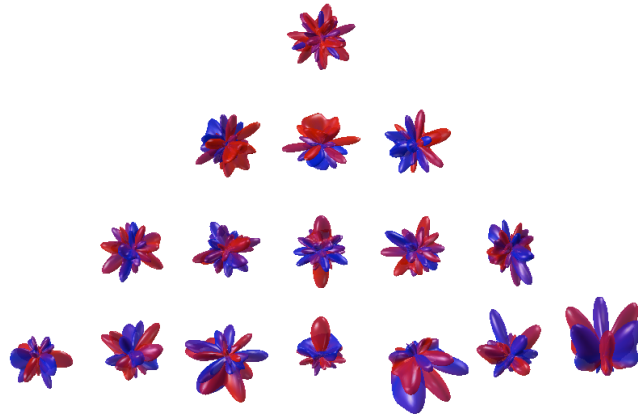
The first 16 SH at r $_a$=1m, f=7500Hz, nmax=30
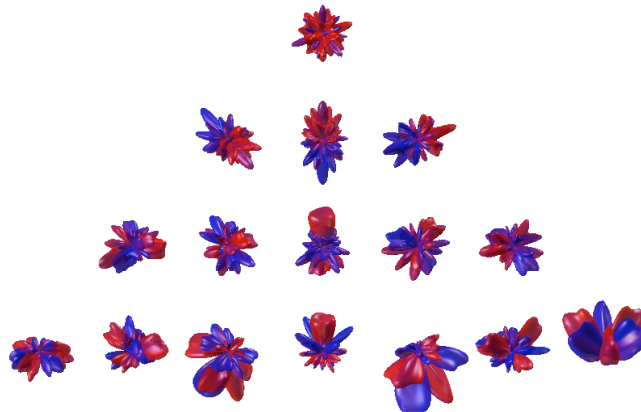
The first 16 SH at r $_a$=1m, f=10000Hz, nmax=30
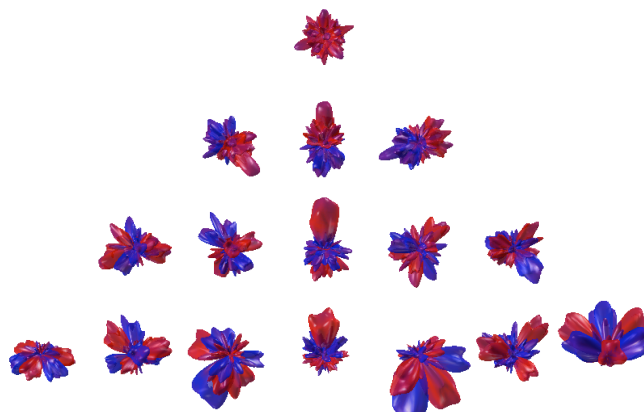
Figure C.2: Truncated subspace calculation

79

Appendix D

Active and Passive Transfer Paths of all 16 Loudspeakers

In chapter 6 the transfer paths are classified by their angular classes. To be able to see, what was measured at each single loudspeaker, here the plots are sorted by their loudspeaker number. Therefore one can detect easily the direct and indirect movements of the membranes. The magnitudes are not normalized to their maximum, rather they show, what was really measured.
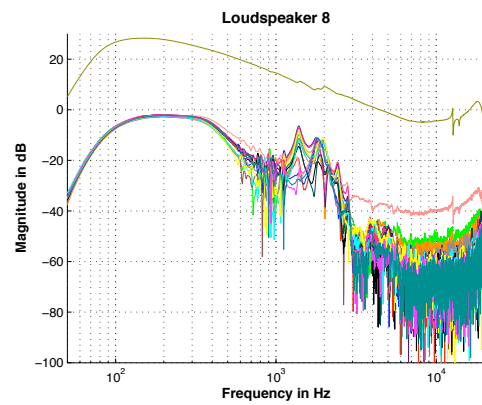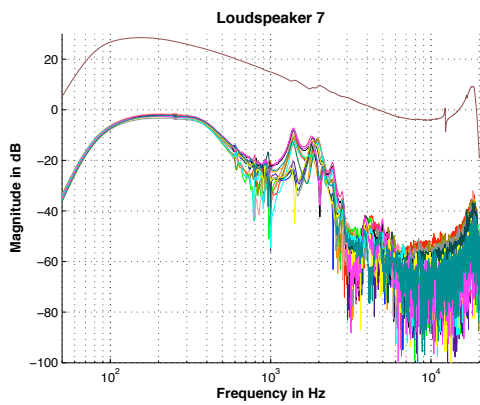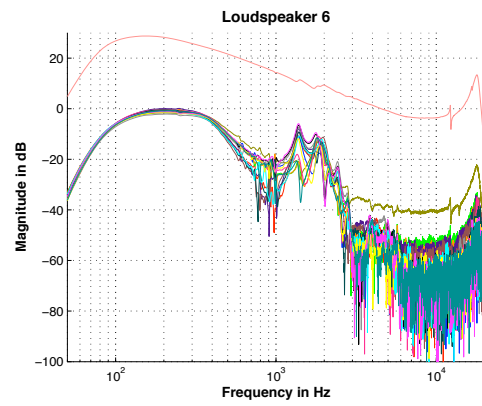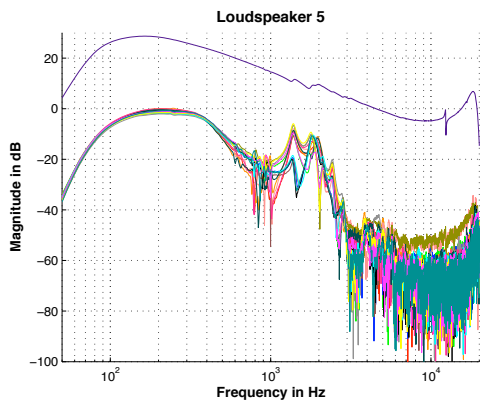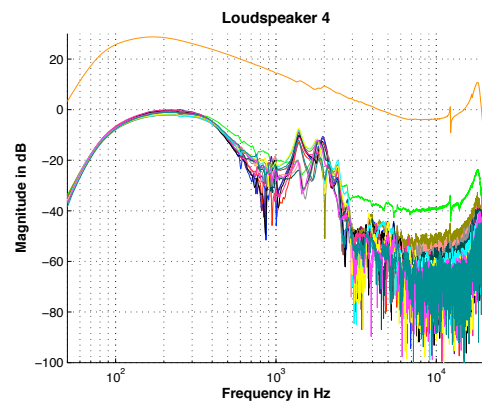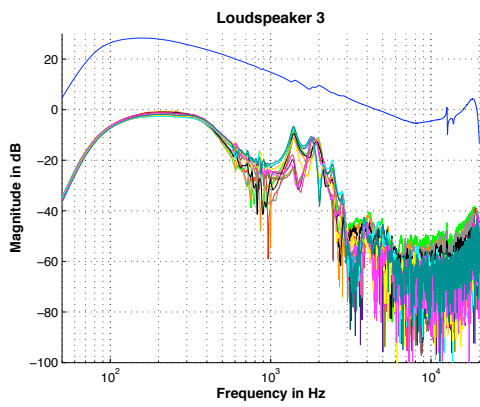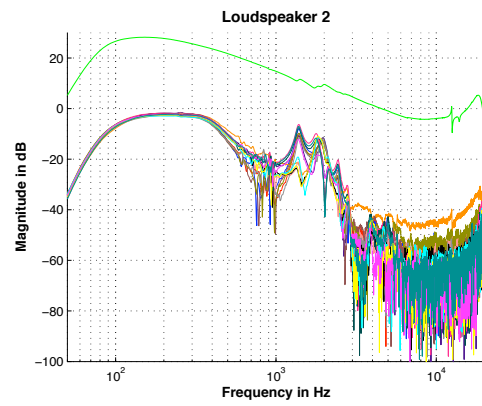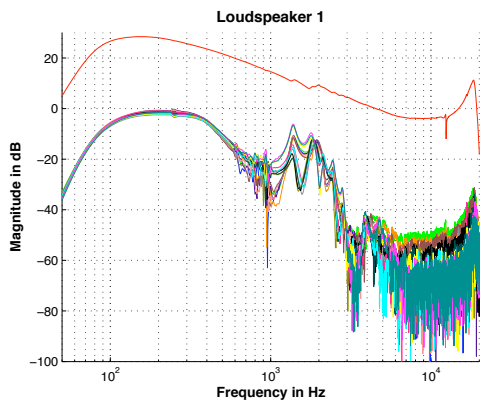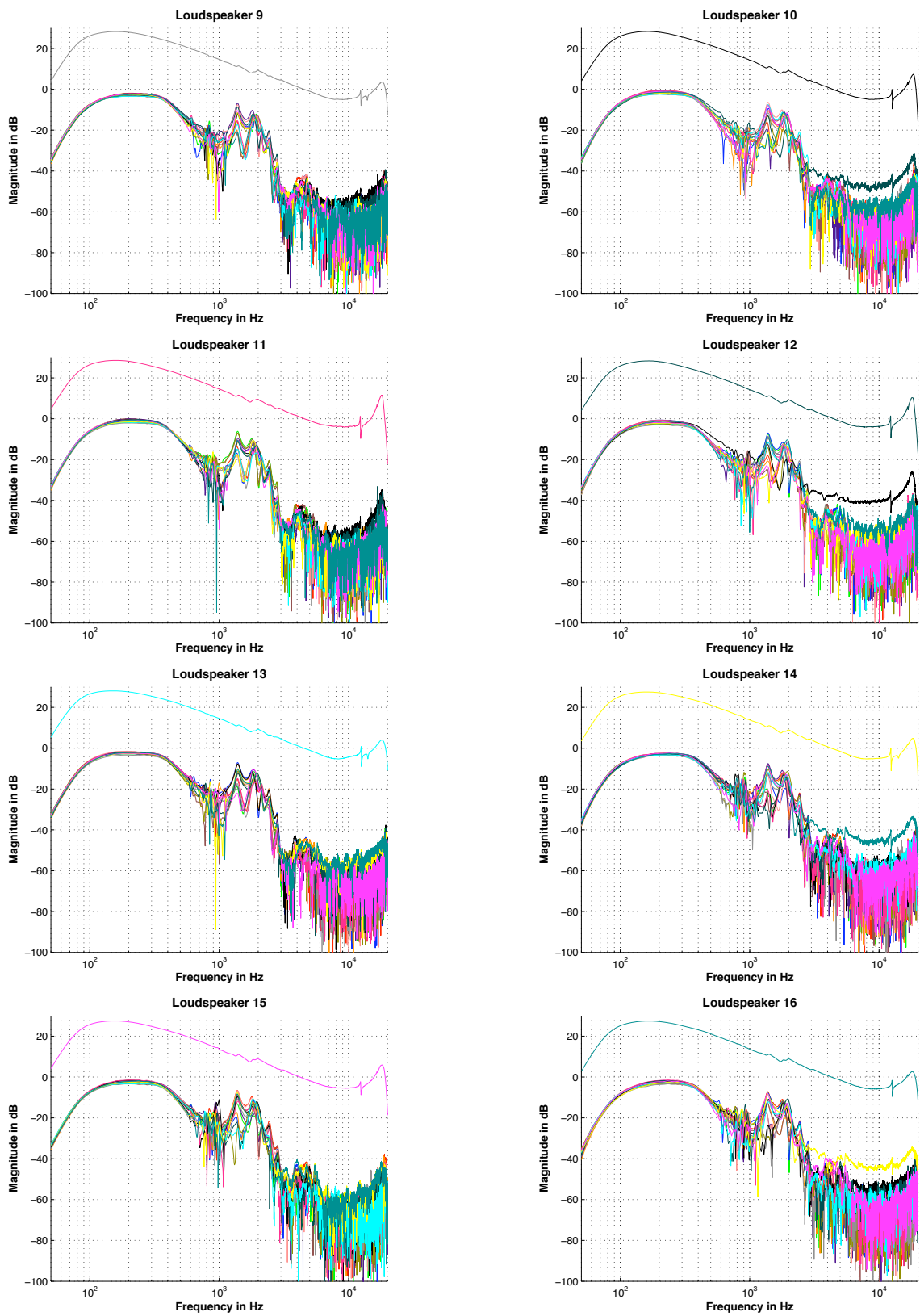
Figure D.1: active and passive frequency responses of all 16 loudspeaker

Bibliography

[Far00]   Angelo Farina. Simultaneous measurement of impulse response and distortion with a swept-sine technique. 2000.

[GW03]   Gerhard Graber and Werner Weselak. *Raumakusitk*. TU Graz, 2003.

[Hoh09]   Fabian Hohl. Kugelmikrophonarray zur Abstrahlungsversmessung von Musikinstrumenten. Master's thesis, KU Graz, 2009.

[HS06]   Kerstin Hesse and Ian Sloan. Hyperinterpolation on the sphere. 2006.

[JR07]   Christian Jochum and Peter Reiner. Erfassung und Evaluierung der Übersprecheigenschaften des Ikosaeder-Lautsprechers. 2007.

[KW04]   Peter Kassakian and David Wessel. Characterization of spherical loudspeaker arrays. 2004.

[LDV]   *Polytec: Portable Digital Vibrometer PDV 100.*

[LW]   Daniel Lichtblau and Eric W. Weisstein. Condition number. www.mathworld.wolfram.com/conditionnumber.

[Maj07]   Piotr Majdak. Algorithmen in Akustik und Computermusik 1: Systemidentifikation. 2007.

[Ort09]   Dieter Ortner. Die fünf platonischen Körper, 2009.

[Ple09]   Peter Plessas. Rigid sphere microphone arrays for spacial recording and holography. Master's thesis, KU Graz, 2009.

[Pol07]   Martin Pollow. Variable directivity of dodecahedron loudspeakers. Master's thesis, Aachen, 2007.

[Pom08]   Hannes Pomberger. Angular and radial directivity control for spherical loud-speaker arrays. Master's thesis, KU Graz, 2008.

[Ren09]   Robert Renka.   Voronoi tesselation with stripack. http://www.math.uni-luebeck.de/keiner/sonstiges.shtml, 2009.

[SW01]   Ian Sloan and Robert Womersley. Extremal systems of points and numerical integration on the sphere. 2001.

[Thy]   Thymphany. *Peerless 830983 2 inch extended range drivers, data sheet.*

[TM07]   Paul Tipler and Gene Mosca. *Physik für Wissenschaftler und Ingenieure.* Elsevier Verlag, 2007.

[Wil99]   Earl G. Wiliams. *Fourier Acoustics.* Academic Press, 1999.

[Wim92]   Lienhard Wimmer. Gleichmäßige Verteilung von Punkten auf der Einheitskugel. Master's thesis, Universität Salzburg, 1992.

[Wom09]   Robert Womersley. Extremal (maximum determinant) points on the sphere. http://web.maths.unsw.edu.au/ rsw/sphere/extremal/index.html, 2009.

[ZH07]   Franz Zotter and Robert Höldrich. Modeling radiation synthesis with spherical loudspeaker arrays. 2007.

[ZN07]   Franz Zotter and Markus Noisternig. Near- and farfield beamforming using spherical loudspeaker arrays. 2007.

[Zot08]   Franz Zotter. Sampling strategies for acoustic holography/ holophony on the sphere. 2008.

[Zot09]   Franz Zotter. *Analysis and Synthesis of Sound-Radiation with Spherical Arrays.* PhD thesis, KU Graz, 2009.

[ZPS08]   F. Zotter, H. Pomberger, and A. Schmeder. Efficient directivity pattern control for spherical loudspeaker arrays. 2008.

[ZSH07]   Franz Zotter, Alois Sontacchi, and Robert Höldrich. Modeling a spherical loudspeaker system as multipole source. 2007.